



# Structural details of amyloid $\beta$ oligomers in complex with human prion protein as revealed by solid-state MAS NMR spectroscopy

Received for publication, September 11, 2020, and in revised form, February 24, 2021. Published, Papers in Press, March 3, 2021.

<https://doi.org/10.1016/j.jbc.2021.100499>

Anna S. König<sup>1,2</sup>, Nadine S. Rösener<sup>1,2</sup>, Lothar Gremer<sup>1,2,3</sup>, Markus Tusche<sup>1</sup>, Daniel Flender<sup>2</sup>, Elke Reinartz<sup>2</sup>, Wolfgang Hoyer<sup>1,2</sup>, Philipp Neudecker<sup>1,2</sup>, Dieter Willbold<sup>1,2,3,\*</sup>, and Henrike Heise<sup>1,2,\*</sup>

From the <sup>1</sup>Institute of Biological Information Processing (IBI-7: Structural Biochemistry) and JuStruct: Jülich Center for Structural Biology, Forschungszentrum Jülich, Jülich, Germany; <sup>2</sup>Institut für Physikalische Biologie, Heinrich-Heine-Universität Düsseldorf, Düsseldorf, Germany; <sup>3</sup>Research Center for Molecular Mechanisms of Aging and Age-Related Diseases, Moscow Institute of Physics and Technology (State University), Dolgoprudny, Russia

Edited by Wolfgang Peti

Human PrP (huPrP) is a high-affinity receptor for oligomeric amyloid  $\beta$  (A $\beta$ ) protein aggregates. Binding of A $\beta$  oligomers to membrane-anchored huPrP has been suggested to trigger neurotoxic cell signaling in Alzheimer's disease, while an N-terminal soluble fragment of huPrP can sequester A $\beta$  oligomers and reduce their toxicity. Synthetic oligomeric A $\beta$  species are known to be heterogeneous, dynamic, and transient, rendering their structural investigation particularly challenging. Here, using huPrP to preserve A $\beta$  oligomers by coprecipitating them into large heteroassemblies, we investigated the conformations of A $\beta$ (1–42) oligomers and huPrP in the complex by solid-state MAS NMR spectroscopy. The disordered N-terminal region of huPrP becomes immobilized in the complex and therefore visible in dipolar spectra without adopting chemical shifts characteristic of a regular secondary structure. Most of the well-defined C-terminal part of huPrP is part of the rigid complex, and solid-state NMR spectra suggest a loss in regular secondary structure in the two C-terminal  $\alpha$ -helices. For A $\beta$ (1–42) oligomers in complex with huPrP, secondary chemical shifts reveal substantial  $\beta$ -strand content. Importantly, not all A $\beta$ (1–42) molecules within the complex have identical conformations. Comparison with the chemical shifts of synthetic A $\beta$  fibrils suggests that the A $\beta$  oligomer preparation represents a heterogeneous mixture of  $\beta$ -strand-rich assemblies, of which some have the potential to evolve and elongate into different fibril polymorphs, reflecting a general propensity of A $\beta$  to adopt variable  $\beta$ -strand-rich conformers. Taken together, our results reveal structural changes in huPrP upon binding to A $\beta$  oligomers that suggest a role of the C terminus of huPrP in cell signaling. Trapping A $\beta$ (1–42) oligomers by binding to huPrP has proved to be a useful tool for studying the structure of these highly heterogeneous  $\beta$ -strand-rich assemblies.

Alzheimer's disease (AD) accounts for an estimated 60 to 80% of all types of dementia (1). One of the hallmarks of AD is the formation of amyloid plaques, which consist mainly of amyloid  $\beta$  (A $\beta$ ) peptides comprising 39 to 43 residues (2). A $\beta$  is produced by cleavage of the amyloid precursor protein (APP) by  $\beta$ - and  $\gamma$ -secretases (3). Of the two most abundant species A $\beta$ (1–40) and A $\beta$ (1–42), the latter is more prone to aggregation and its aggregates are more toxic (3). Small to moderately sized A $\beta$  oligomers (A $\beta$ <sub>oligo</sub>) have been identified as the most neurotoxic factor in the pathogenesis of AD, whereas large fibrils are known to be the main component of insoluble plaques (4). Detailed structural information on A $\beta$ (1–42)<sub>oligo</sub> is thus of paramount interest, and in recent years, structural studies on different oligomer preparations of A $\beta$ (1–42)<sub>oligo</sub>, A $\beta$ (1–40)<sub>oligo</sub> (5, 6) (or pyro-Glu-A $\beta$ (3/11–40) oligomers (7)) by solid-state NMR-spectroscopy have been conducted (8–15). Shape, morphology, and structural details of those oligomers were strongly dependent on preparation conditions, and while all of these oligomers had a high prevalence of  $\beta$ -strand secondary structure, tertiary fold and supramolecular arrangement of  $\beta$ -strands were found to differ strongly between different preparations. While in most mature fibrils  $\beta$ -strands are arranged in parallel in-register  $\beta$ -sheets (16, 17), quaternary structures in oligomers are much more variable, and, depending on the fibrillation pathway, parallel (12), antiparallel (18)  $\beta$ -sheets or even a mixture of both (11) have been found. A major challenge to structural studies of oligomers is their transient nature, and thus, most oligomer preparations exhibit substantial structural heterogeneity. Stabilization of oligomers is essential for long-term structural investigations. In most cases, further aggregation of oligomers was prevented by freeze-trapping with subsequent lyophilization (7–12, 14). In this study, we used the recombinant human prion protein in its native cellular prion protein (PrP<sup>C</sup>) conformation to trap A $\beta$  oligomers by coprecipitating them into large heteroassemblies, in which the growth of A $\beta$ <sub>oligo</sub> is prevented, as demonstrated by long-term solid-state NMR measurements over 11 months.

The PrP<sup>C</sup> is a high-affinity cell-surface receptor for A $\beta$ <sub>oligo</sub> (19, 20), and PrP<sup>C</sup> is also able to bind to fibrillar A $\beta$  (21–23). It

\* For correspondence: Dieter Willbold, [d.willbold@fz-juelich.de](mailto:d.willbold@fz-juelich.de); Henrike Heise, [h.heise@fz-juelich.de](mailto:h.heise@fz-juelich.de).

Present address for Daniel Flender: Institut für Mikrobiologie, Universität Greifswald, Greifswald, Germany.

## Solid-state MAS NMR of the complex of huPrP and A $\beta$ <sub>oligo</sub>

has been suggested that binding of A $\beta$ <sub>oligo</sub> to membrane-anchored PrP<sup>C</sup> mediates A $\beta$  toxicity during AD by mediating synapse damage (24) and the blockade of long-term potentiation by A $\beta$ <sub>oligo</sub> (19, 25) *via* activation of Fyn-kinase pathways (26, 27) (Fig. S1), but this has also been questioned (28–31). It has also been described that soluble PrP (32) and its N-terminal fragment PrP(23–111) (33, 34) have a protective role by inhibiting A $\beta$  fibrillation and sequestration of A $\beta$ <sub>oligo</sub>.

Several *in vitro* studies on the A $\beta$ -PrP interaction suggest that A $\beta$ <sub>oligos</sub> bind at two Lys-rich parts (residues 23–27 and  $\approx$ 95–110) on PrP (35–40), but an additional involvement of the C terminus of PrP has also been suggested (21). Interestingly, the N terminus of human PrP is also able to bind oligomeric  $\alpha$ -synuclein with high affinity (41–43). A structural study of insoluble PrP<sup>C</sup>-A $\beta$ <sub>oligo</sub> complexes described them as a “hydrogel,” in which the A $\beta$ (1–42)<sub>oligos</sub> were rigid, while PrP still has high molecular mobility (44). Additionally, this study reported a conformational change in the N terminus of PrP<sup>C</sup> upon complexation with A $\beta$ <sub>oligo</sub>. We recently demonstrated that A $\beta$ <sub>oligo</sub> forms large heteroassemblies with either full-length (huPrP(23–230)) or C-terminally truncated (huPrP(23–144)) membrane-anchorless monomeric PrP (40). These assemblies have a size of a few micrometers as determined by dynamic light scattering and show cloud-like morphologies as seen by atomic force microscopy (40). The A $\beta$ :huPrP stoichiometry of the heteroassemblies depends on the amount of huPrP added to A $\beta$ <sub>oligo</sub> and reaches a value of 4:1 (monomer ratio A $\beta$ :huPrP) if either huPrP(23–144) or huPrP(23–230) is added to the oligomer solution in excess (40). In all these *in vitro* preparations, A $\beta$  oligomers and early-stage protofibrils are stabilized and prevented from elongation by PrP, which has been shown to preferentially bind to fast-growing fibril and oligomer ends (22).

Here we exploit this stabilizing effect in an NMR study on different samples of A $\beta$ <sub>oligo</sub> complexed by huPrP. Isotope labeling of either huPrP or A $\beta$  allowed us to characterize both components of the complex separately. While the N-terminal region of huPrP in the complex remains largely devoid of secondary structure and still undergoes fast backbone conformational averaging on the microsecond to millisecond timescale, A $\beta$ <sub>oligos</sub> exhibit a high degree of  $\beta$ -strand conformation. While these A $\beta$ <sub>oligos</sub> are highly heterogeneous, solid-state NMR spectra reveal similarities with the corresponding spectra of all fibril polymorphs published so far (45–47).

## Results

### **The N-terminal construct huPrP(23–144) is disordered in solution at mildly acidic and neutral pH**

The solution structure of huPrP(23–230) had originally been determined in acetate buffer at an acidic pH of 4.5 and a temperature of 20 °C (48), whereas the huPrP-A $\beta$ (1–42)<sub>oligo</sub> complex samples for solid-state NMR were prepared at a pH value close to neutral. As a basis for studying the interaction between huPrP and A $\beta$ <sub>oligo</sub>, we therefore first investigated free huPrP(23–144) by NMR spectroscopy in solution at different pH values ranging from 4.5 to 7.0 and at a temperature of

5.0 °C, which is closer to the temperature used for the solid-state NMR experiments. As reported previously, the chemical shifts of the N-terminal amino acid residues 23 to 124 in truncated huPrP(23–144) are almost identical to those of huPrP(23–230), whereas residues 125 to 144, which are part of the well-ordered globular domain of huPrP(23–230), are strongly affected by the truncation at position 144 (40).

We obtained almost complete sequence-specific <sup>1</sup>H, <sup>13</sup>C, and <sup>15</sup>N backbone resonance assignments for huPrP(23–144) at pH values of 4.5 and 7.0 and a temperature of 5.0 °C using a combination of HNC0, HNCACB, and BEST-TROSY-(H) N(COCA)NH triple-resonance experiments (Fig. S2). The assigned chemical shifts at pH 4.5 and pH 7.0 have been deposited with the Biological Magnetic Resonance Data Bank (BMRB) under accession codes 28115 and 28116, respectively.

As expected, side-chain titration in this pH range causes significant chemical shift changes for all seven histidine residues and for residues next to histidine. Other than that, the chemical shifts at pH 4.5 and pH 7.0 are very similar to each other and very close to random coil shifts (49). Quantitative analysis reveals that the Random Coil Index (RCI) order parameters (50)  $S_{RCI}^2$ , which are a measure of how different the backbone chemical shifts are from those of a disordered random coil on a scale of 0 (typical for a random coil) to 1 (typical for a well-ordered backbone conformation), are consistently below  $\approx$ 0.6 (Fig. S3). This demonstrates conclusively that free huPrP(23–144) in solution at neutral and mildly acidic pH is highly disordered and devoid of any stable secondary structure.

### **The flexible N terminus of huPrP becomes immobilized but remains almost devoid of regular secondary structure upon binding to A $\beta$ <sub>oligo</sub>**

High-molecular-weight heteroassemblies of oligomeric A $\beta$ (1–42) and huPrP(23–144) or of oligomeric A $\beta$ (1–42) and huPrP(23–230) were prepared by adding the respective huPrP construct to a preincubated solution of A $\beta$ (1–42), as described previously (40). Immediately after addition of huPrP to the solution, precipitation of a solid fine white powder was observed.

These formed high-molecular-weight heteroassemblies were analyzed by an MTT cell viability test (Fig. 1A). Both huPrP(23–230) and huPrP(23–144) reduce A $\beta$ (1–42)<sub>oligo</sub> toxicity in a concentration-dependent manner, thus these complexes are not toxic, and huPrP has a protective effect. As our complexes do not exhibit a GPI anchor, this fits to the observation of a protective role for non-membrane-bound huPrP fragments (32, 36) in contrast to membrane-anchored huPrP, which mediates neurotoxicity (19, 24, 25). The fragment huPrP(121–230), which was shown to not form any heteroassemblies (40), however, does not rescue A $\beta$ (1–42)<sub>oligo</sub> toxicity and was used as a negative control. None of the huPrP fragments alone is toxic for the cells (Fig. 1A).

High-molecular-weight assemblies of A $\beta$ (1–42)<sub>oligo</sub> and huPrP(23–144) were further analyzed by sucrose density gradient ultracentrifugation (DGC) and subsequent SDS-

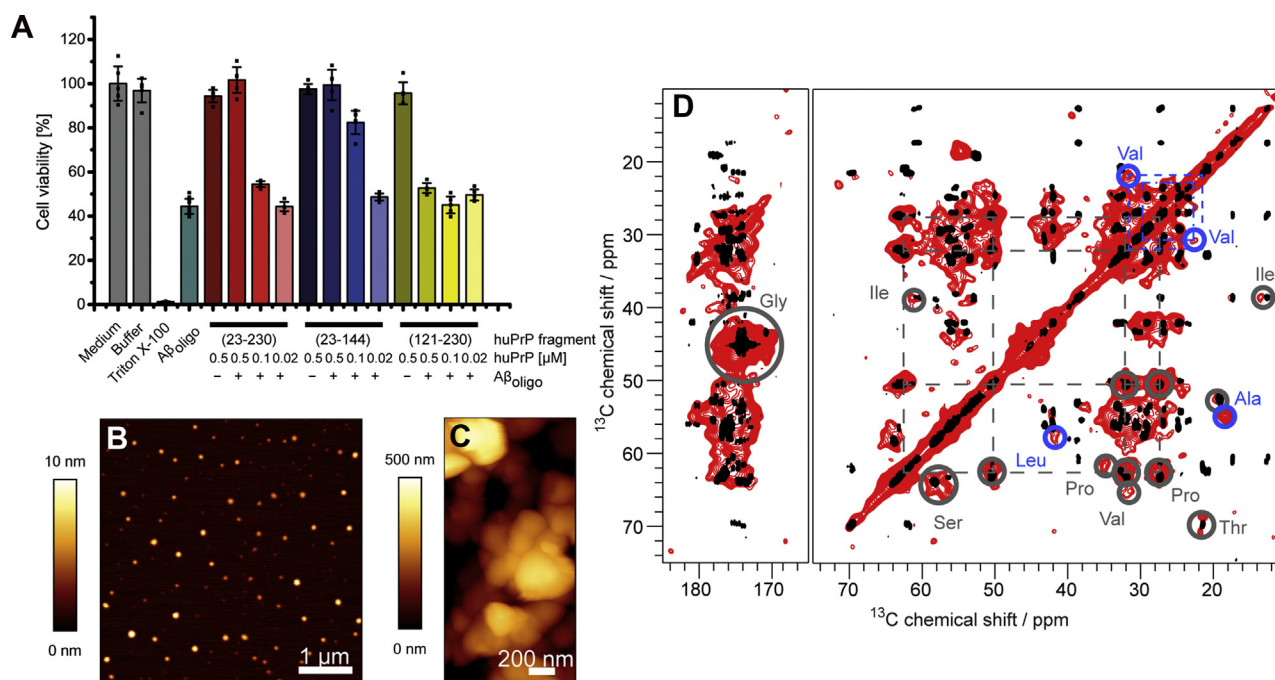


**Figure 1.** **A**, MTT assay of 1  $\mu$ M A $\beta$ <sub>oligo</sub> and of 1  $\mu$ M A $\beta$ <sub>oligo</sub> in complex with either 0.5  $\mu$ M, 0.1  $\mu$ M, or 0.02  $\mu$ M of either huPrP(23-230), huPrP(23-144) or huPrP(121-230). Both huPrP(23-230) and huPrP(23-144) reduce A $\beta$ <sub>oligo</sub> toxicity in a concentration-dependent manner. In contrast, the C-terminal fragment huPrP(121-230) does not. None of the huPrP fragments alone reduces cell viability. This reduction of toxicity has been seen for non-membrane-bound huPrP fragments before (32, 36) and is in contrast to toxic effects of membrane-anchored huPrP (19, 24, 25). As our complexes do not exhibit a GPI-anchor, the reduction of toxicity reflects these observations. **B**, 5  $\mu$ m  $\times$  5  $\mu$ m AFM image of 440 nM A $\beta$ <sub>oligo</sub> and **C**, 2  $\mu$ m  $\times$  1  $\mu$ m AFM image of A $\beta$ <sub>oligo</sub>-huPrP(23-144) coprecipitates generated with 80  $\mu$ M preincubated A $\beta$ (1-42) and 40  $\mu$ M huPrP(23-144). The aggregates have sizes up to 1  $\mu$ m spanning clusters with a smooth surface appearance, whereas A $\beta$ <sub>oligo</sub> are small nm spheres. **D**, comparison of a PDS D spectrum of monomeric huPrP(23-144)-A $\beta$  (\* species is  $^{13}$ C,  $^{15}$ N uniformly labeled) in red with a  $^{13}$ C- $^{13}$ C TOCSY spectrum of monomeric huPrP(23-144) in black. The PDS D spectrum was recorded at a temperature of  $\approx$ -6  $^{\circ}$ C, a spinning frequency of 11 kHz and a mixing time of 30 ms and the TOCSY spectrum at a temperature of 5.0  $^{\circ}$ C, at pH 6.7. Gray circles indicate some identified amino acid types, dashed lines Pro and Val connections in the PDS D spectrum. Due to broad line widths and a low signal dispersion in the PDS D spectrum several correlations overlap, especially for the residues in the octarepeat region. Nevertheless, spin systems for most of the amino acid types present in the sequence could be identified and an amino-acid-type specific resonance assignment was possible. Differences between the PDS D and TOCSY spectrum are highlighted with blue circles. For an additional PDS D spectrum see Fig. S6, the corresponding double quantum-single quantum correlation spectrum (DQ-SPC5) is shown in Fig. S7.

PAGE and RP-HPLC (40) (Fig. S4). As previously described (40), a molar ratio of A $\beta$ :PrP of 4:1 is obtained in the assemblies if huPrP is added in excess; for higher A $\beta$ :PrP ratios, not all potential PrP-binding sites on A $\beta$ <sub>oligo</sub> are saturated with huPrP(23-144) (as in sample huPrP(23-144)-A $\beta$ \*, \* indicates that the A $\beta$  moiety of the complex is  $^{13}$ C,  $^{15}$ N labeled).

In Figure 1 typical AFM images of A $\beta$ <sub>oligo</sub> alone (Fig. 1B) or in complex with N-terminal huPrP(23-144) (Fig. 1C) are shown. Spherical A $\beta$  oligomers can clearly be identified (Fig. 1B), and no fibrils are observed in the huPrP(23-144)-A $\beta$  condensates (Fig. 1C). Next, we focused on investigating structural features of the complex by NMR spectroscopy.

To probe the flexibility of the N-terminal construct huPrP(23-144) in the complex, we recorded a  $^1$ H- $^{13}$ C insensitive nuclei enhanced by polarization transfer (INEPT)-NMR spectrum as well as dipolar-based  $^1$ H- $^{13}$ C and  $^1$ H- $^{15}$ N cross polarization (CP)-MAS spectra (51). The INEPT-NMR spectrum of this sample did not show any protein signals at a sample temperature of  $\approx$ 27  $^{\circ}$ C (spectrum not shown), whereas in  $^1$ H- $^{13}$ C (recorded at a sample temperature of  $\approx$ 0  $^{\circ}$ C) and  $^1$ H- $^{15}$ N CP spectra (recorded at a sample temperature of  $\approx$ -6  $^{\circ}$ C) strong signals typical for all amino acid types can be seen (Fig. S5). This indicates that huPrP(23-144) in complex with A $\beta$ (1-42)<sub>oligo</sub> is

immobilized and does not undergo rapid isotropic reorientation as in solution.

In Figure 1D a typical 2D  $^{13}$ C- $^{13}$ C-correlation spectrum obtained with proton-driven spin-diffusion (PDS D) of huPrP(23-144)\*-A $\beta$  (\* indicates that the huPrP moiety of the complex is  $^{13}$ C,  $^{15}$ N labeled) is overlaid with a  $^{13}$ C- $^{13}$ C total correlation spectrum (TOCSY) of monomeric huPrP(23-144) in solution at pH 6.7. Except for some Val and Ala resonances, most of the peaks align well. This indicates that the natively unfolded N terminus of huPrP does not undergo a major conformational rearrangement upon complex formation with A $\beta$ <sub>oligo</sub>, but conformational averaging of backbone conformations is still possible on the microsecond to millisecond timescale. Due to the lack of secondary structure in the intrinsically unstructured N terminus as well as the repetitiveness of the amino acid sequence in the octarepeats, the signal overlap is so severe that sequence-specific resonance assignment for the solid-state NMR spectra was not possible.

While most of the resonances of huPrP(23-144) in complex with A $\beta$ <sub>oligo</sub> have the same chemical shifts as huPrP(23-144) in solution, some differences can be clearly seen; in particular, some Ala, Val, and Leu resonances are shifted from random coil toward  $\alpha$ -helical secondary chemical shifts. Six out of seven Ala residues

## Solid-state MAS NMR of the complex of huPrP and A $\beta$ <sub>oligo</sub>

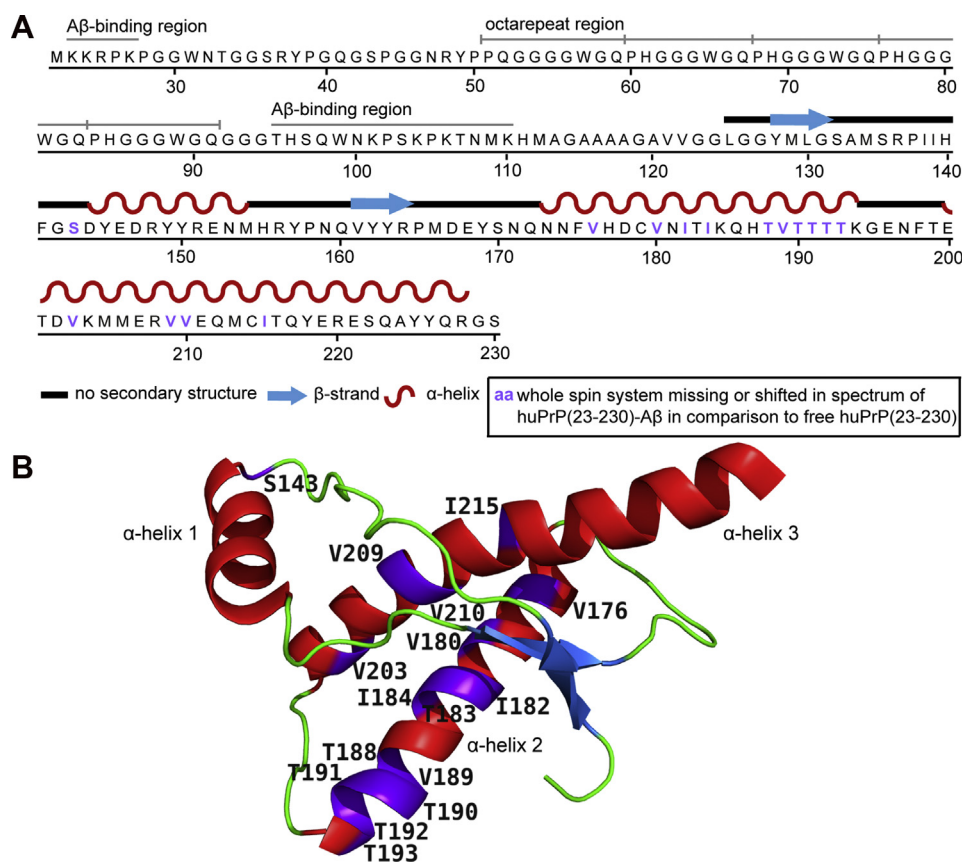


**Figure 2. A, amino acid sequence of huPrP(23–230) (48) used in this study.** The A $\beta$ -binding regions K23–K27 and T95–K110 (35–40) and the five octarepeats are indicated above the sequence. **B, 3D structure of the natively folded prion domain (residues 125–228) of full-length huPrP(23–230) in solution.**  $\beta$ -strands are colored blue,  $\alpha$ -helices red. Picture adapted from PDB-File 1QLZ (48). Residues whose entire spin system is missing or shifted in the PDS spectra (Figs. S10–S12) are highlighted in purple in A and B.

as well as both Val and Leu residues present in the sequence are located within a short stretch from residue 113 to 130, a region that starts with the so-called palindrome segment (A<sup>113</sup>GAAAAGA<sup>120</sup>) (see Fig. 2A). Thus, structural changes upon complexation with A $\beta$ <sub>oligo</sub> in N-terminal huPrP(23–144) seem to be confined mainly to the region between A113 and L130.

These findings are also supported by analysis of secondary chemical shifts (Fig. S8). Most secondary chemical shifts of huPrP(23–144) in solution are random coil chemical shifts indicative of a lack of regular secondary structure. Likewise, most spin systems of huPrP(23–144) in complex with A $\beta$ <sub>oligo</sub> are typical random coil chemical shifts, with some  $\alpha$ -helical shifts found for Ala, Leu, and Val, which are not found for monomeric huPrP(23–144). Notably, almost no  $\beta$ -strand-like secondary chemical shifts were identified for complexed huPrP(23–144). This finding is an indication that huPrP(23–144) did not aggregate into amyloid fibrils. We also compared the chemical shifts of huPrP(23–144) fibrils (52, 53) with our correlation spectrum of huPrP(23–144)\*-A $\beta$  (Fig. S9A). Most of the signals observed for fibrillar huPrP(23–144) do not overlap with the signals in our huPrP(23–144)\*-A $\beta$  spectra. We therefore conclude that the conformations of huPrP(23–144) in huPrP(23–144)\*-A $\beta$  and the huPrP(23–144) fibril are very different, and the interaction with A $\beta$ <sub>oligo</sub> did not induce huPrP(23–144) fibril formation.

### The C terminus of huPrP shows changes in $\alpha$ -helices 2 and 3 upon A $\beta$ <sub>oligo</sub> binding

For full-length huPrP in complex with A $\beta$ <sub>oligo</sub>, huPrP(23–230)\*-A $\beta$  (see Table 1), no signals were detected at  $\approx 30$  °C in the INEPT spectrum (not shown), which indicates that not only the N terminus, but also the C terminus of huPrP is not highly dynamic. By contrast, excitation with <sup>1</sup>H-<sup>13</sup>C CP results in a typical <sup>13</sup>C NMR spectrum expected for a protein. To test whether the full protein is visible in the spectrum or whether a substantial part of the protein is too mobile for dipolar transfer, we compared 1D spectra obtained with <sup>13</sup>C direct excitation (DE) and <sup>1</sup>H-<sup>13</sup>C CP spectra recorded at sample temperatures of  $\approx 30$ , 10, and  $-10$  °C (Fig. 3). At all three temperatures, no substantial differences between the

**Table 1**  
 Details of the samples used for the solid-state NMR measurements (\* species is <sup>13</sup>C, <sup>15</sup>N uniformly labeled)

| Sample                                    | <sup>13</sup> C, <sup>15</sup> N labeled species | Monomer stoichiometry A $\beta$ :huPrP (initial mixture) | Monomer stoichiometry A $\beta$ :huPrP (in complexes) |
|---|--|--|---|
| huPrP(23–144)*-A $\beta$                  | huPrP(23–144)                                    | 6:1  | not estimated   |
| huPrP(23–230)*-A $\beta$                  | huPrP(23–230)                                    | 4:1  | not estimated   |
| huPrP(23–144)-A $\beta$ *                 | A $\beta$ (1–42)                                 | 8:1  | 8.6:1   |
| huPrP(23–144) <sub>exc</sub> -A $\beta$ * | A $\beta$ (1–42)                                 | 2:1  | (3.7 $\pm$ 0.12):1                                    |

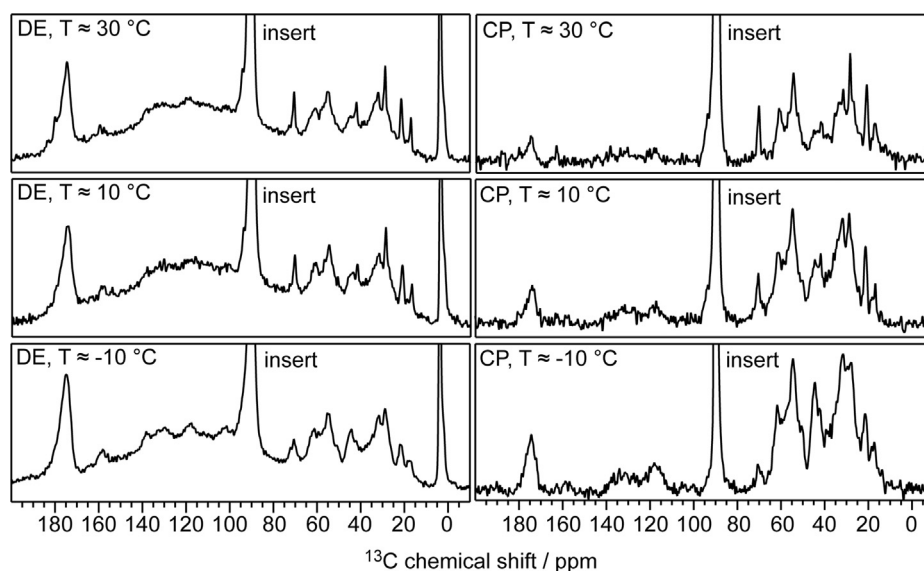


**Figure 3.**  $^{13}\text{C}$  Direct excitation (DE) and  $^1\text{H}$ - $^{13}\text{C}$  CP spectra of huPrP(23–230)\*-A $\beta$  (\* species is  $^{13}\text{C}$ ,  $^{15}\text{N}$  uniformly labeled) recorded at temperatures of  $\approx 30$ , 10, and  $-10$  °C and 11 kHz spinning frequency. Recycle delays of 20 s and 2 s were used for DE and  $^1\text{H}$ - $^{13}\text{C}$  CP experiments, respectively. The signal at 90 ppm is caused by the rotor insert (Delrin) and is cut off for clarity. The signal at around 0 ppm in the  $^{13}\text{C}$  DE spectrum belongs to a silicone-based rotor inlet and is likewise cut off for clarity, the broad bump centred at 120 ppm however is the Teflon background of the probe. Both signals are not detected in the CP spectra. Signal intensities were scaled to the number of scans for each spectrum. Even at the lowest temperature the free water in the sample was not completely frozen, as verified by  $^1\text{H}$  spectra (not shown).

spectra are visible. Signal intensities in both types of spectra are roughly proportional to  $1/T$  following Curie's law, and at all temperatures signal intensities in CP spectra are up to two times higher than in the respective DE spectra. This is an indication that the complete huPrP molecule is fully immobilized over the whole temperature range and does not undergo major mobility changes (44). Some signals (e.g.,  $\approx 70$  ppm,  $\text{C}_\beta$  of Thr) show broader linewidths at lower temperatures, indicating reduced motional averaging of chemical shifts.

In Figure 4, a typical 2D PDSM spectrum of the huPrP(23–230)\*-A $\beta$  complex is displayed. A line width of  $\approx 1$  ppm is observed for the  $^{13}\text{C}$  resonances, and due to the large number of resonances and the limited signal dispersion, the signal overlap is so substantial that a sequential resonance assignment or even a quantitative analysis of residue-specific correlations was not possible. Nevertheless, a comparison with the corresponding 2D  $^{13}\text{C}$ - $^{13}\text{C}$  correlation spectrum of the N-terminal construct huPrP(23–144) in complex with oligomeric A $\beta$  (red outline in Fig. 4) allows some conclusions about the structure of full-length complexed huPrP: First, almost all resonances observed in the spectrum of C-terminally truncated huPrP(23–144) appear to be also visible in the spectrum of full-length huPrP(23–230)\*-A $\beta$  (Fig. 4). These findings suggest that the C terminus of full-length huPrP(23–230) does not have a major impact on the conformation of the N terminus and its interaction with A $\beta$ <sub>oligo</sub>, in line with previous results (35–37, 40). Second, the spectrum of full-length huPrP complexed by A $\beta$ <sub>oligo</sub> displays additional resonances, which are absent in the spectrum of N-terminal huPrP(23–144) in complex with A $\beta$ <sub>oligo</sub>. Some of the amino acid residues occurring mainly in the C terminus (e.g., Ile, Thr, and Val) give rise to cross peaks that can be unambiguously

identified in 2D  $^{13}\text{C}$ - $^{13}\text{C}$  correlation spectra. However, for most C-terminal amino acid residues (e.g., Asp, Glu, Tyr, etc., Fig. 2A), the 2D correlations overlap with other resonances and can therefore not be unambiguously assigned.

We compared our 2D  $^{13}\text{C}$ - $^{13}\text{C}$  correlation spectrum with the expected correlations between the chemical shifts obtained experimentally for natively folded full-length huPrP in solution

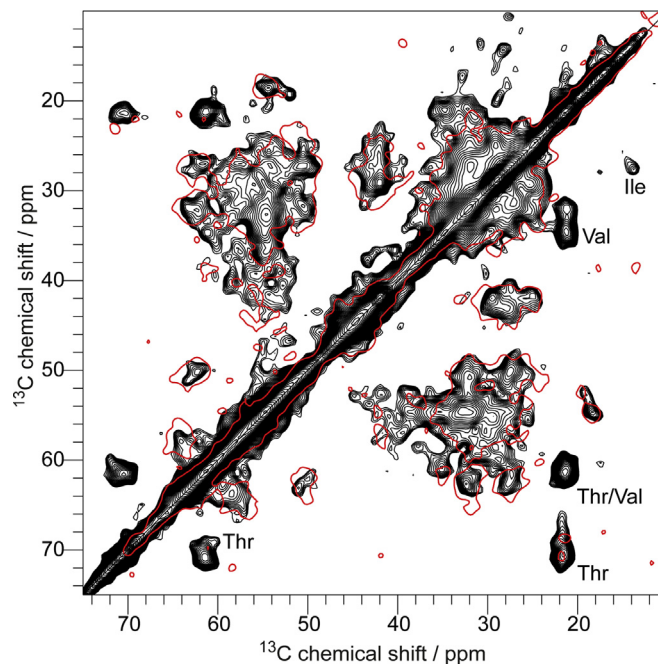


**Figure 4.** Comparison of two PDSM spectra of huPrP(23–230)\*-A $\beta$  (\* species is  $^{13}\text{C}$ ,  $^{15}\text{N}$  uniformly labeled), shown in black, and huPrP(23–144)\*-A $\beta$ , shown as red contour. Both spectra were recorded at a spinning frequency of 11 kHz and a mixing time of 30 ms, but the black one at a temperature of  $\approx 0$  °C and the red one at  $\approx -6$  °C.

## Solid-state MAS NMR of the complex of huPrP and A $\beta$ <sub>oligo</sub>

at pH 4.5 (48). While the predicted N-terminal cross peaks (residues 23–124) superimpose well with the spectrum of huPrP(23–230)\*-A $\beta$ , some discrepancies between the experimental and the predicted spectrum are observed for the C terminus (residues 125–230) (Fig. S10).

In particular, correlation signals for Ile, Thr, and Val in  $\alpha$ -helical conformation from  $\alpha$ -helices 2 and 3 in natively folded huPrP are completely missing in the experimental spectrum (Fig. S11). Instead, correlation signals for Thr and Val with secondary chemical shifts indicative of  $\beta$ -strands that are not observed in natively folded huPrP are clearly visible in the experimental spectrum (Figs. S10–S12). This suggests that at least for a substantial fraction of the huPrP molecules within the complex, some parts of a region between either V121 and I139 and/or V176 and I215 (located in  $\alpha$ -helices 2 and 3) have undergone some structural rearrangements including  $\beta$ -strand formation (Fig. 2B). We could not see any fibril formation in huPrP(23–230) within the complexes; nevertheless, we overlaid our spectrum with predicted peaks for two recently published fibrils from huPrP and its fragment huPrP(94–178). The huPrP(94–178) fibril structure exhibits a  $\beta$ -strand in the palindrome region (54), which is likewise not supported by our  $\alpha$ -helical-like Ala chemical shifts (Fig. S9B). However, a fibril structure recently published for full-length huPrP (55) (see Fig. S9C) shows a lot of similarities to our spectrum especially for Thr and Val residues, suggesting a rearrangement of the C terminus to more  $\beta$ -sheet-like chemical shifts.

### High $\beta$ -strand content of A $\beta$ <sub>oligo</sub> in huPrP(23–144)-A $\beta$ complexes

We also investigated the homogeneity and structural characteristics of A $\beta$ <sub>oligo</sub> using two samples containing uniformly  $^{13}\text{C}$ ,  $^{15}\text{N}$  labeled A $\beta$ <sub>oligo</sub> in complex with nonlabeled huPrP(23–144) in two different molar ratios (Table 1). In the first sample (indicated as huPrP(23–144)-A $\beta$ \*), the molar ratio between A $\beta$  monomers and huPrP was roughly 8:1, whereas in the second preparation (indicated as huPrP(23–144)<sub>exc</sub>-A $\beta$ \*), addition of huPrP(23–144) in excess to the A $\beta$  oligomers resulted in a molar ratio of  $\approx$ 4:1.

INEPT spectra recorded at  $\approx$ 20 °C of both samples are devoid of protein signals (not shown), whereas  $^1\text{H}$ - $^{13}\text{C}$  and  $^1\text{H}$ - $^{15}\text{N}$  CP spectra recorded at  $\approx$ 0 °C display strong signals typical for all amino acid residue types (Fig. S13). These findings indicate that also the A $\beta$  molecules are rigid in the complex. In all 2D and 3D homonuclear  $^{13}\text{C}$ - $^{13}\text{C}$  and heteronuclear  $^{15}\text{N}$ - $^{13}\text{C}$  correlation spectra (see Fig. 5 and Figs. S14–S18), linewidths are rather broad (0.9 ppm for  $^{13}\text{C}$  and 3.3 ppm for  $^{15}\text{N}$ ), which is an indication for conformational heterogeneity of the A $\beta$  molecules within the complex. In 2D  $^{13}\text{C}$ - $^{13}\text{C}$  correlation spectra (Fig. 5 and Fig. S14),  $^{13}\text{C}$  side chain and backbone resonances can be identified for almost every amino acid residue type in the sequence. For several amino acid residue types, the number of distinct spin systems visible in the spectra is larger than the number of amino acid residues of this type in the amino acid sequence. For example, six Ala spin systems have been found although the sequence of A $\beta$ (1–42)

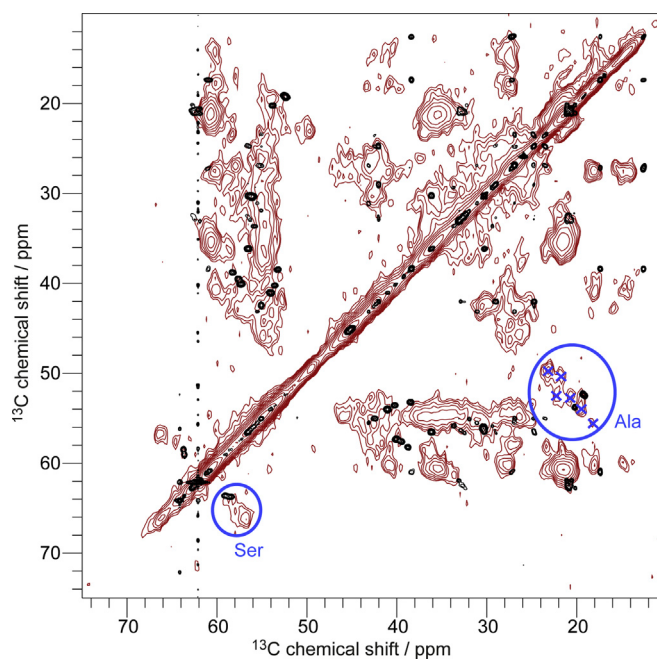


**Figure 5.** Overlay of a PDS D spectrum of huPrP(23–144)-A $\beta$ \* (\* species is  $^{13}\text{C}$ ,  $^{15}\text{N}$  uniformly labeled), measured at a temperature of  $\approx$ 0 °C, a spinning frequency of 11 kHz and a mixing time of 50 ms, in red with a  $^{13}\text{C}$ - $^{13}\text{C}$  TOCSY spectrum of uniformly  $^{13}\text{C}$ ,  $^{15}\text{N}$  isotope labeled A $\beta$  monomers in solution (measured at a temperature of 5.0 °C and pH 7.2 in 30 mM Tris-HCl buffer) in black (the strong resonances at 62.1 ppm and 64.2 ppm with the  $t_1$  noise are from the Tris buffer). Ala and Ser  $\text{C}_\alpha$ - $\text{C}_\beta$  peaks are highlighted with blue circles and six identified Ala spin systems are shown with blue crosses. Chemical shift differences for both residue types between the A $\beta$  monomers (typical random coil chemical shifts) and huPrP(23–144)-A $\beta$ \* ( $\beta$ -strand-like conformations) can be observed.

only contains four Ala residues (Fig. 5). This means that not all A $\beta$  molecules within the complex experience identical environments.

A comparison between a solid-state NMR  $^{13}\text{C}$ - $^{13}\text{C}$  correlation spectrum of A $\beta$ <sub>oligo</sub> in complex with huPrP(23–144) and a  $^{13}\text{C}$ - $^{13}\text{C}$  TOCSY correlation spectrum of A $\beta$  monomers in solution (Fig. 5) reveals strong chemical shift differences and thus indicates that the A $\beta$  monomer building blocks in oligomers have undergone significant structural changes upon oligomerization. While all signals of the solution spectrum have chemical shifts indicative of a random coil, a strong shift to chemical shifts indicative of  $\beta$ -strand-like secondary structure is observed for almost all spin systems of A $\beta$ <sub>oligo</sub> in the spectrum of the complex. For  $\text{C}_\alpha/\text{C}_\beta$  cross peaks of Ala, Ile, Ser, and Val (Fig. 5) in  $\alpha$ -helical, unstructured, and  $\beta$ -strand-like conformations, a quantification was possible by integration of the peak regions (see Fig. S19). Hence, these residues are predominantly in a  $\beta$ -strand conformation. For Gly, which is a  $\beta$ -strand breaker, CO/ $\text{C}_\alpha$  cross peaks are mainly indicative of random coil conformation.

Due to conformational heterogeneity, inhomogeneous line broadening, and substantial resonance overlap in the  $^{13}\text{C}$ - $^{13}\text{C}$  and  $^{15}\text{N}$ - $^{13}\text{C}$  spectra, a full sequential resonance assignment for A $\beta$ <sub>oligo</sub> in complex with huPrP was not possible. However, from a series of PDS D spectra with different mixing times as well as 2D and 3D NCACX and NCOCX spectra, it was

possible to identify some interresidual correlations and to obtain site-specific assignments for some parts of A $\beta$  in one predominant conformation (Table S1). However, it is not clear whether all assigned resonances belong to one type of conformer or to different conformers.

To elucidate whether the stoichiometry of A $\beta$  and huPrP in the heteroassemblies has an influence on the conformations of A $\beta$  molecules, we prepared and investigated a second sample, in which huPrP(23–144) was added in excess to <sup>13</sup>C, <sup>15</sup>N labeled A $\beta$ <sub>oligo</sub>. In this sample, all potential huPrP-binding sites on A $\beta$ <sub>oligo</sub> should be occupied. Overall there is not much difference between sample huPrP(23–144)-A $\beta$ \* and huPrP(23–144)<sub>exc</sub>-A $\beta$ \* in a PDS spectrum with a mixing time of 50 ms, except for minor changes (Fig. S20). As there are no major structural changes upon altering the huPrP concentration, we conclude that the conformational heterogeneity is not due to unoccupied huPrP-binding sites in A $\beta$ <sub>oligo</sub>, but rather A $\beta$ <sub>oligos</sub> in complex with huPrP consist of inequivalent conformers and/or A $\beta$ <sub>oligo</sub> assemblies are different from each other.

## Discussion

In this study we investigated the interaction of A $\beta$ (1–42)<sub>oligo</sub> and huPrP by solid-state NMR spectroscopy. As mentioned above, A $\beta$ (1–42)<sub>oligo</sub> play a crucial role in AD, as they are neurotoxic (4). Determining structural information of A $\beta$ (1–42)<sub>oligo</sub> is challenging because of their transient and fast-aggregating nature. Therefore, trapping A $\beta$ (1–42)<sub>oligo</sub> with huPrP and inhibiting their aggregation is a convenient way to study their structure. The interaction between A $\beta$ (1–42)<sub>oligo</sub> and huPrP has also a role in AD: Nieznanski *et al.* and others showed that soluble huPrP is able to inhibit A $\beta$  fibril formation (32, 56), particularly the naturally secreted huPrP fragment N1 (huPrP(23–111)) (33, 34) and sequesters toxic A $\beta$ (1–42)<sub>oligo</sub> (32). Additionally, soluble huPrP reduces the toxic effects of A $\beta$ (1–42)<sub>oligo</sub>, as seen by us (see Fig. 1A and (40)) and others (32, 36).

Aside from the protective role of soluble huPrP in AD, membrane-anchored huPrP is mediating neurotoxicity of A $\beta$ (1–42)<sub>oligo</sub> (19, 24, 25) *via* Fyn-kinase (26, 27) or NMDA receptor pathways (57). Although A $\beta$ (1–42)<sub>oligo</sub> toxicity is not solely dependent on huPrP (28–31), it has been shown that especially small A $\beta$ (1–42)<sub>oligo</sub> (58) and high-molecular-weight A $\beta$ (1–42)<sub>oligo</sub> (59, 60) mediate toxicity by huPrP. To target this interaction efficient inhibitors might prevent A $\beta$ (1–42)<sub>oligos</sub>' detrimental effects. Indeed, A $\beta$ (1–42)<sub>oligo</sub>-binding D-enantiomeric peptides (40, 61) and antibodies (19, 62–64) have been shown to efficiently block the interaction between huPrP and A $\beta$ (1–42)<sub>oligo</sub>, but more efficient inhibitors are needed. The process of research for efficient inhibitors will be speeded up by detailed knowledge of the binding between A $\beta$ (1–42)<sub>oligo</sub> and huPrP in terms of structure, because targeted research and rational design of either huPrP- or A $\beta$ (1–42)<sub>oligo</sub>-binding agents will be possible.

In this study, high-molecular-weight aggregates were formed by addition of N-terminal or full-length human PrP to preformed A $\beta$ (1–42)<sub>oligos</sub>. These aggregates formed immediately

upon addition of huPrP, visible as the precipitation of a fine white solid powder. The rigidity of this complex was further confirmed by DE and CP NMR spectra recorded at different temperatures (see Fig. 3).

In a previous study, Kostylev *et al.* (44) investigated complexes formed between huPrP(23–111) or huPrP(23–230) and oligomeric Met-A $\beta$ (1–42). In that study, the complexes were described as a hydrogel, and PrP molecules exhibited a higher degree of flexibility. The difference between their and our complexes may be explained by differences in the preparation of the complex (different buffer system), and in particular of the A $\beta$  oligomers, which consisted of  $\approx$ 12 molecules in the study of Kostylev *et al.* and of on average  $\approx$ 23 monomers (61) in our study, which most certainly has an effect on their oligomer structure. Also, the A $\beta$ (1–42) species used by Kostylev *et al.* contained an additional methionine residue at the N terminus, which could lead to different behavior of the A $\beta$ (1–42) oligomers, although Silvers *et al.* (65) could show that Met-A $\beta$ (1–42) and A $\beta$ (1–42) fibrils exhibit the same aggregation kinetics and, except for a slight change in flexibility of the N terminus, are structurally comparable. Additionally, Kostylev *et al.* (44) used huPrP(23–111) for the majority of their investigations, whereas we used a slightly longer construct (huPrP(23–144)). This could also account for the different physical behavior in terms of flexibility.

As just mentioned, we did most of the investigations on an N-terminal construct of huPrP (huPrP(23–144)) for the following reasons: Firstly, the N terminus of huPrP is sufficient for binding A $\beta$ (1–42)<sub>oligo</sub>, as shown by us (40) and others (35–39). Further, using huPrP(23–144) instead of huPrP(23–230) drastically reduces signal overlap in the spectra making it more straightforward to draw conclusions for the N terminus. The naturally secreted soluble N1 fragment (although slightly shorter: 23–111) exhibits a protective role in AD by reducing the cytotoxicity of A $\beta$ (1–42)<sub>oligo</sub> (34). We could show by MTT toxicity tests that also our construct huPrP(23–144) as well as soluble full-length huPrP(23–230) significantly reduced A $\beta$ (1–42)<sub>oligo</sub> toxicity (Fig. 1A). From a comparison of 2D <sup>13</sup>C-<sup>13</sup>C spectra, we could show that the C terminus of huPrP(23–230) has no impact on the binding of the N terminus (23–144) to A $\beta$ (1–42)<sub>oligo</sub>, suggesting that the protective effect of soluble huPrP is linked to the N terminus of huPrP. Therefore, the different roles of huPrP in the etiology of AD (*i.e.*, mediation of neurodegeneration *versus* neuroprotection) might be rather attributed to the place of action (membrane-anchored *versus* soluble) than to the length of the protein.

All the findings of this study are summarized in a schematic representation of the structural features of the huPrP-A $\beta$ <sub>oligo</sub> complex in Figure 6. The N-terminal region of huPrP is rigid but has no regular secondary structure in the complex with A $\beta$ <sub>oligo</sub>. This is the case for both analyzed huPrP constructs. Minor structural changes to more  $\alpha$ -helical-like secondary structure are restricted to a region between A113 and L130, including the palindrome region AGAAAAGA. This palindrome, known as the “hydrophobic core,” is highly conserved and highly amyloidogenic (66). The palindrome segment has

## Solid-state MAS NMR of the complex of huPrP and A $\beta$ <sub>oligo</sub>

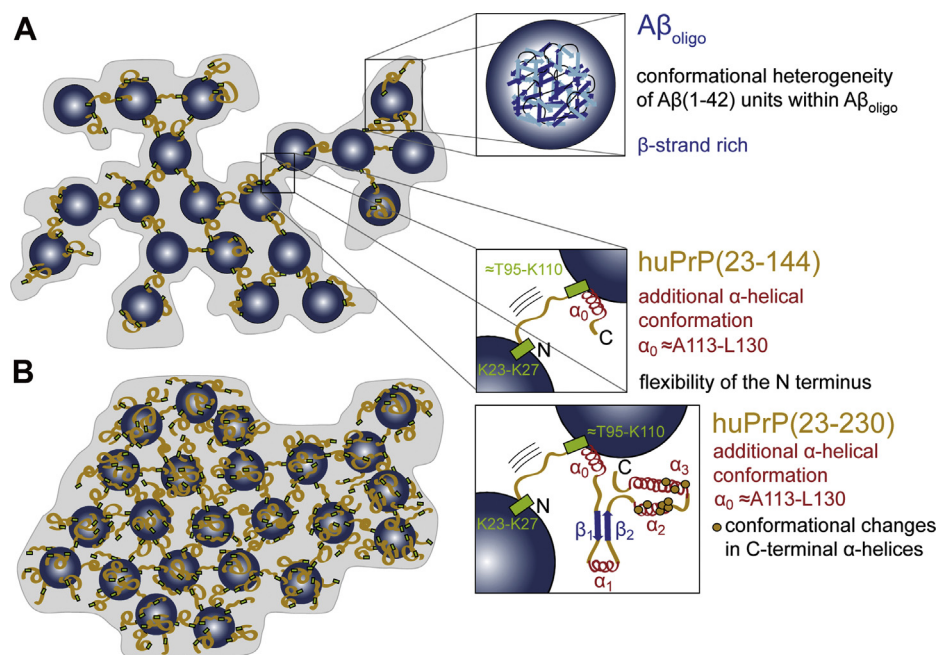


**Figure 6. Schematic representation showing structural features of the huPrP-A $\beta$ <sub>oligo</sub> complex for A, low huPrP content as in the sample where huPrP(23-144) is not in excess (huPrP(23-144)-A $\beta^*$ ) and B, with high huPrP content as in the sample where huPrP(23-144) was added in excess (huPrP(23-144)<sub>exc</sub>-A $\beta^*$ ). huPrP is shown as orange lines, A $\beta$ <sub>oligo</sub> as blue spheres,  $\alpha$ -helices are red, and  $\beta$ -strands blue. Binding regions at huPrP are shown as light green boxes, conformational changes in the C terminus of huPrP as orange dots. Picture adapted from Rösener *et al.* (40).**

previously been suggested to be required for the attainment of the PrP<sup>Sc</sup> conformation and to facilitate the proper association of PrP<sup>Sc</sup> with PrP<sup>C</sup> to enable prion propagation (67). Trapping the “hydrophobic core” by binding to A $\beta$ (1-42)<sub>oligo</sub> might explain the A $\beta$ (1-42)-oligomer-induced inhibition of prion propagation proposed by Sarell *et al.* (68). In the already discussed above study of a hydrogel-termed complex of full-length huPrP and A $\beta$ <sub>oligo</sub> (44), the formation of two additional  $\alpha$ -helices, one in the octarepeat region (residues 51-91) and one in the palindrome segment (A<sup>113</sup>GAAAAGA<sup>120</sup>), was postulated from the observation that chemical shifts observed for Gly and Ala are predominantly  $\alpha$ -helical in their spectra (44). Our results support the formation of the latter  $\alpha$ -helix in the complex with full-length huPrP. Chemical shifts of Gly residues as well as all other N-terminal residues are predominantly random coil-like in the spectra (see Fig. 1D), suggesting that the octarepeat region does not undergo major structural rearrangements upon complex formation. These differences are explainable by the different preparation conditions and huPrP and A $\beta$ (1-42)<sub>oligo</sub> constructs used as stated above.

For full-length huPrP in complex with A $\beta$ <sub>oligo</sub> we observed some changes for Thr and Val residues from  $\alpha$ -helical to random coil or even  $\beta$ -strand-like secondary chemical shifts compared with well-folded monomeric huPrP in solution (48). The residues affected by these chemical shift changes are mainly located in  $\alpha$ -helices 2 and 3, thus suggesting that the helical structure of this region is at least partially lost in complex with A $\beta$ <sub>oligo</sub>. For huPrP in a hydrogel with A $\beta$ <sub>oligo</sub> chemical shift changes from  $\alpha$ -helical to random coil values were also described for Thr residues, which are mainly located in  $\alpha$ -helices 2 and 3 (44). This observation was attributed to a loss of secondary structure during liquid-liquid phase

separation of PrP and in the complex with A $\beta$ <sub>oligo</sub>. The loss of secondary structure in the complex with A $\beta$ <sub>oligo</sub> is confirmed by us. This observed change in secondary structure in the C-terminal domain of PrP<sup>C</sup> upon binding to A $\beta$  oligomers suggests that also the C-terminal domain of PrP<sup>C</sup> interacts with A $\beta$ <sub>oligo</sub>. On the contrary, the C-terminal domain is not able to bind A $\beta$ <sub>oligo</sub> on its own (40), so chemical shift changes in the C terminus might be some type of steric hindrance, a disfavor of  $\alpha$ -helical conformations in close proximity to the  $\beta$ -strand-like A $\beta$ <sub>oligo</sub> or simply a structural change induced by binding of A $\beta$ <sub>oligo</sub> to the N terminus. As we could show that A $\beta$ <sub>oligo</sub> and the C-terminal fragment huPrP(121-230) do not form high-molecular-weight aggregates (40) and that this huPrP fragment does not reduce A $\beta$ <sub>oligo</sub> cytotoxicity (see Fig. 1A), a direct binding of A $\beta$ <sub>oligo</sub> and the C terminus of huPrP is rather unlikely. Consequently the C terminus is free to interact with any secondary (transmembrane) receptors necessary for the signal transduction, because PrP<sup>C</sup> itself is no transmembrane protein and therefore requires a secondary receptor, such as NMDAR (57) or the metabotropic glutamate receptor 5 (mGluR5) (69) to facilitate A $\beta$ <sub>oligo</sub>-induced neurotoxicity. Indeed the A $\beta$ <sub>oligo</sub>-PrP<sup>C</sup>-mGluR5 complex has been shown to mediate neurotoxic Fyn-kinase pathways: Um *et al.* demonstrated that the interaction between membrane-anchored full-length PrP<sup>C</sup> and mGluR5 is stabilized by A $\beta$ <sub>oligo</sub>. This interaction in turn enables binding to Fyn-kinase and leads to the subsequent Fyn-kinase cascade and independent of that to increased calcium influx into the cell (69). Additionally, the A $\beta$ <sub>oligo</sub>-PrP<sup>C</sup>-mGluR5 complex enables NMDA and muscarinic-acetylcholine receptor-independent long-term depression (70) and modulates the binding to intracellular proteins (71). It might be attractive to speculate that these interactions are

mediated by a structural change in the C terminus of PrP<sup>C</sup>. This has to be further investigated. In another study (21), PrP constructs encompassing the N-terminal but lacking the C-terminal domain were inactive in inhibiting A $\beta$  polymerization, even though they still bound to fibrils, whereas full-length PrP<sup>C</sup> completely inhibited fibril elongation. This implied that the C-terminal domain might play some role in inhibiting polymerization. It is thus tempting to speculate that the conformational transition of the C-terminal domain to more  $\beta$ -strand-like structures could also be due to the incorporation into a fibril equivalent surface on A $\beta$  oligomers. This is also supported by the finding that the C-terminal chemical shifts of huPrP overlap well with a recently published full-length huPrP fibril structure (55) (see Fig. S9C). Nevertheless, we should keep in mind that other studies following the aggregation of A $\beta$  in presence of different huPrP constructs suggested the N terminus necessary for inhibiting A $\beta$  aggregation (32, 36, 39) and also our own data argue against a direct binding of A $\beta$ <sub>oligo</sub> to the C terminus of huPrP (40), as stated above.

A $\beta$ <sub>oligo</sub> in complex with huPrP consists of nonidentical A $\beta$  conformers. This is not surprising given the fact that the complex of huPrP(23–144) and A $\beta$ <sub>oligo</sub> contains four times more A $\beta$  (monomer equivalent) than huPrP(23–144) molecules (40). Not every monomer within the oligomer (containing  $\approx$ 23 monomer units on average (61)) might be able to bind to huPrP(23–144) in the same way and has therefore the same conformation (40), as described above. These nonidentical conformers can have different origins: (i) different types of monomers within the oligomer, because not every monomer can bind to huPrP (A $\beta$ -huPrP *versus* A $\beta$ -A $\beta$  interactions); (ii) polymorphism within the oligomer independent of the binding to huPrP (iii) polymorphism between different oligomers; or (iv) a combination thereof.

The secondary structure of A $\beta$ <sub>oligo</sub> in complex with huPrP shows a high degree of  $\beta$ -strand content. Because we took care not to obtain any fibrils in our samples during preparation (see exemplarily Fig. 1C) and because there were no major chemical shift changes in the CP and PDSM spectra in the following 11 months (during which the sample was kept at temperatures between 4 °C and 8 °C), it is very unlikely that any significant amount of fibrils might have formed over time. Instead, the high degree of  $\beta$ -strand content indicates that A $\beta$ <sub>oligos</sub> already contain A $\beta$  monomer units that have at least in part the same secondary structure as in fibrils or protofibrils, but probably differ in tertiary structure. This phenomenon has already been observed in early stage A $\beta$  oligomers (8, 72) and is supported by the finding that huPrP-mediated toxicity depends partially on high-molecular-weight fibrillar-like A $\beta$ <sub>oligo</sub> (59, 60). Assuming that the A $\beta$ <sub>oligo</sub> preparation yielded a heterogeneous collection of fibril-like conformers in terms of secondary structure, of which most if not all were obviously elongation incompetent when trapped by adding huPrP, one would expect that the solid-state NMR resonances of A $\beta$ <sub>oligo</sub> in complex with huPrP are the sum of the resonances of different fibril conformations together with resonances from A $\beta$  units that experience different environments due to edge effects and/or huPrP interaction. To assess the structural similarity of A $\beta$ <sub>oligo</sub> with fibrils and protofibrils, we superimposed all available

resonances from three different A $\beta$ (1–42) fibril types (45–47) and one artificial protofibril (13) with the PDSM spectrum of A $\beta$ <sub>oligo</sub> in complex with huPrP (Fig. 7 and Figs. S21–S24). A large fraction of the predicted correlations from these different protofibril and fibril types are represented by correlation peaks in our oligomer spectra, with some minor deviations found for Ala correlations. These findings suggest that the A $\beta$ <sub>oligo</sub> preparation represents a heterogeneous mixture of  $\beta$ -strand-rich assemblies, of which some may have the potential to evolve into the different fibril types when not trapped by huPrP. The conformational heterogeneity of A $\beta$ <sub>oligo</sub> is closely related to the polymorphism of A $\beta$  fibrils and reflects the general propensity of A $\beta$  to adopt variable  $\beta$ -structure conformers. Although we did not directly detect the binding site on A $\beta$ <sub>oligo</sub>, our data suggest that the high  $\beta$ -strand content might be necessary for the binding, as monomers, which do not show  $\beta$ -strand content, have no or only little affinity for huPrP (35, 73). A $\beta$  fibrils do bind PrP (20), but with much lower affinity than A $\beta$ <sub>oligo</sub>. This might be due to the different tertiary structure compared with A $\beta$ <sub>oligo</sub>. This hypothesis is also supported by others, who assume that a 3D structure rather than a special part of the sequence is necessary for binding, as elucidated by epitope mapping (37).

The propensity of huPrP to efficiently bind to A $\beta$ <sub>oligo</sub> and to “freeze” them in a nondynamic and nonelongating state allowed us to investigate the conformers of A $\beta$ <sub>oligo</sub> and the huPrP moiety by NMR over several months without noticeable changes in the sample. It is tempting to speculate whether this property of huPrP is a coincidence, or whether it is part of the long-sought function of PrP. Regardless of whether PrP inhibits elongation of A $\beta$  oligomers and fibrils or whether PrP is a mediator of cytotoxicity of A $\beta$ <sub>oligos</sub>, substances that compete with PrP for A $\beta$ <sub>oligo</sub> binding and which thus can do the same

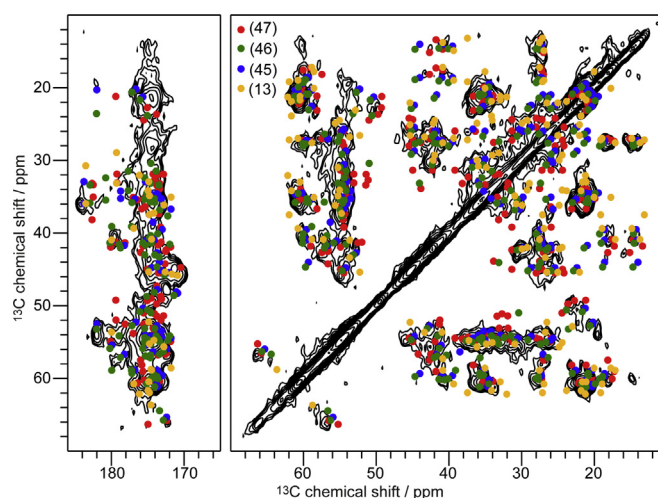


**Figure 7.** A PDSM spectrum (measured at a temperature of  $\approx$ 0 °C, a spinning frequency of 11 kHz and a mixing time of 50 ms, same spectrum as in Fig. 5) of huPrP(23–144)-A $\beta$ \* (\* species is <sup>13</sup>C, <sup>15</sup>N uniformly labeled) in comparison with predicted cross peaks (up to two bonds) for three different fibril types, which are obtained at pH values of 2 (red) (47) or 7.4 (green (46) and blue (45)) and an artificial protofibril (yellow) (13). Separate overlays of this PDSM spectrum with spectra of these fibrils are shown in Figs. S21–S24.

## Solid-state MAS NMR of the complex of huPrP and A $\beta$ <sub>oligo</sub>

job without the potential of mediating cytotoxicity may be of high therapeutic potential.

### Experimental procedures

#### Proteins

##### A $\beta$

For preparation of NMR samples with unlabeled A $\beta$ , synthetic A $\beta$ (1–42) obtained from Bachem AG was used. (For preparation of stocks see below.) Uniformly <sup>13</sup>C, <sup>15</sup>N labeled A $\beta$ (1–42) was purchased from Isoloid GmbH.

##### huPrP

The purification of recombinant full-length huPrP(23–230) and C-terminally truncated huPrP(23–144) either unlabeled or uniformly <sup>13</sup>C, <sup>15</sup>N labeled, and of recombinant unlabeled huPrP(121–230) was performed as described previously (40).

#### Preparation of A $\beta$ (1–42) stocks

Synthetic unlabeled A $\beta$ (1–42) (Bachem AG, 1 mg aliquot) was incubated with 700  $\mu$ l hexafluoro-2-propanol (HFIP) overnight and divided into 108  $\mu$ g doses in LoBind reaction tubes (Eppendorf AG). Samples were lyophilized in a rotational vacuum concentrator system connected to a cold trap (both Martin Christ Gefriertrocknungsanlagen GmbH). The lyophilizates were stored at room temperature and protected from light.

#### Preparation of high-molecular-weight heteroassemblies from amyloid $\beta$ oligomers and different human prion protein constructs in different molar ratios

For sample preparation, A $\beta$ (1–42) lyophilizates (either uniformly <sup>13</sup>C, <sup>15</sup>N labeled or unlabeled) were dissolved in 30 mM Tris-HCl buffer, pH 7.4, yielding A $\beta$ (1–42) concentrations of 160–300  $\mu$ M. After 2 h of incubation at 22 °C and 600 rpm shaking to obtain A $\beta$ <sub>oligo</sub>, either huPrP(23–144) or huPrP(23–230) was added to yield concentrations of 40 to 80  $\mu$ M within the initial mixture leading to the molar ratios mentioned in Table 1. The addition of huPrP resulted in immediate sedimentation of the complex as a powder-like precipitate (40).

After addition of 0.03% of sodium azide and incubation for 30 min, the samples were centrifuged for 2 to 5 min at 16,100g, and the supernatant was removed. The sediment was washed twice with up to 2 ml of 30 mM Tris-HCl buffer, 0.03% sodium azide, pH 7.4 to remove excess monomeric PrP. After removal of the supernatant, the samples were transferred into 3.2 mm MAS rotors with a Hamilton syringe and centrifuged. In total, four different samples were prepared in which either huPrP or A $\beta$ (1–42) was uniformly <sup>13</sup>C, <sup>15</sup>N labeled, using different huPrP constructs and molar ratios between huPrP and A $\beta$ (1–42) (Table 1).

#### Characterization by density gradient ultracentrifugation, SDS-PAGE, and RP-HPLC

For biophysical characterization of e.g., sample huPrP(23–144)-A $\beta$ <sup>\*</sup>, sucrose density gradient

ultracentrifugation (DGC) was performed. To this end, 10  $\mu$ l of the sedimented but unwashed sample was diluted with 90  $\mu$ l of 30 mM Tris-HCl buffer, pH 7.4 and applied on a discontinuous sucrose gradient (see (40)) and centrifuged for 3 h at 259,000g and 4 °C. After fractionation, each of the 14 fractions was analyzed by Tris-Tricine SDS-PAGE and RP-HPLC as previously described (40) (Fig. S4).

RP-HPLC revealed the A $\beta$ :huPrP(23–144) stoichiometry shown in Table 1 as determined in a single measurement. Sample huPrP(23–144)<sub>exc</sub>-A $\beta$ <sup>\*</sup> was not separated by DGC but measured by RP-HPLC and revealed an A $\beta$ :huPrP(23–144) stoichiometry of 3.7  $\pm$  0.12 to 1 after fivefold measurement of the same sample. All stoichiometries represent monomer equivalents.

#### MTT cell viability tests

Potential cell viability rescue of rat pheochromocytoma PC-12 cells (Leibniz Institute DSMZ) from A $\beta$ (1–42)<sub>oligo</sub>-induced toxicity through addition of soluble huPrP(23–144), huPrP(23–230), or huPrP(121–230) in a concentration-dependent manner was measured in MTT (3-(4,5-dimethylthiazol-2-yl)-2,5-diphenyltetrazolium bromide) cell viability tests (40, 61).

PC-12 cells were cultivated in RPMI 1640 medium supplemented with 10% fetal calf serum and 5% horse serum, seeded (10,000 cells in 100  $\mu$ l per well) on collagen-coated 96-well plates (Gibco, Life Technologies), and incubated in a 95% humidified atmosphere with 5% CO<sub>2</sub> at 37 °C for 24 h. Then final concentrations of 1  $\mu$ M A $\beta$ (1–42)<sub>oligo</sub> either in the absence or after mixing and further incubation for 30 min at 22 °C with 0.02, 0.1, or 0.5  $\mu$ M (final concentrations) of the respective huPrP protein were added. In addition, the toxicity of the respective huPrP proteins alone at 0.5  $\mu$ M final concentrations was also determined.

After further incubation in a 95% humidified atmosphere with 5% CO<sub>2</sub> at 37 °C for 24 h, cell viability was measured using the Cell Proliferation Kit I (MTT) (Roche Applied Science) according to manufacturer's protocol. The MTT formazan product was determined by measuring the absorbance at 570 nm corrected by subtraction of the absorbance at 660 nm in a FluoroStar Optima plate reader (BMG Labtech). The arithmetic mean of five independent measurements per approach  $\pm$ SD was calculated. All results were normalized to untreated cells grown in medium only.

#### AFM measurements

The samples used for AFM were either A $\beta$ (1–42)<sub>oligo</sub> or A $\beta$ (1–42)<sub>oligo</sub> complexed by huPrP(23–144).

For formation of A $\beta$ (1–42)<sub>oligo</sub>, monomeric A $\beta$ (1–42) was incubated at a concentration of 80  $\mu$ M in 30 mM Tris-HCl, pH 7.4 for 2.5 h at 22 °C and 600 rpm shaking. For AFM the sample was then diluted to 0.44  $\mu$ M with buffer and 50  $\mu$ l of the solution was transferred to freshly cleaved mica and incubated for 30 min at room temperature for mica adhesion.

Preparation of the A $\beta$ (1–42)<sub>oligo</sub>-huPrP(23–144) sample was done as follows: Monomeric A $\beta$ (1–42) at a concentration of

120  $\mu$ M in 30 mM Tris-HCl, pH 7.4 was incubated for 2 h, 22 °C and 600 rpm shaking. Then huPrP(23–144) was added leading to a final concentration of 80  $\mu$ M A $\beta$ (1–42) and 40  $\mu$ M huPrP(23–144) in the sample. The sample was incubated further for 30 min. The generated precipitates are cleared from possibly unbound A $\beta$ (1–42) or huPrP(23–144) by centrifugation at 16,100g and 4 °C for 30 min. The pellet containing the pure A $\beta$ (1–42)<sub>oligo</sub>-huPrP(23–144) precipitate was washed twice with 100  $\mu$ l 30 mM Tris-HCl, pH 7.4 with centrifugation steps at 16,100g in between. After resuspension of the condensates in 100  $\mu$ l of 30 mM Tris-HCl, pH 7.4, then 50  $\mu$ l of the sample was incubated on freshly cleaved mica for 30 min.

All samples were washed three times with MilliQ water and dried in a gentle stream of N<sub>2</sub>. Both samples were measured in a Nanowizard 3 system (JPK Instruments AG) using intermittent contact mode with a resolution of 1024 pixels and line rates of 0.5 to 1 Hz in ambient conditions with a silicon cantilever with nominal spring constant of 26 N/m and average tip radius of 7 nm (Olympus OMCL-AC160TS). Due to the curvature and adhesion of the A $\beta$ (1–42)<sub>oligo</sub>-huPrP(23–144) condensates, the imaging parameters (amplitude, setpoint, and gain) had to be adapted slightly and the cantilever had to be changed often. The height image of A $\beta$ (1–42)<sub>oligo</sub> was flattened with the JPK Data Processing software 5.0.69.

#### Preparation of solution NMR samples

For the sequence-specific backbone resonance assignments, samples of 0.36 mM uniformly <sup>13</sup>C, <sup>15</sup>N labeled huPrP(23–144) with 50 mM sodium acetate buffer in 10% (v/v) D<sub>2</sub>O (pH 4.5) and 0.30 mM uniformly <sup>13</sup>C, <sup>15</sup>N labeled huPrP(23–144) with 50 mM HEPES buffer in 10% (v/v) D<sub>2</sub>O (pH 7.0) were prepared as reported previously (Rösener *et al.* (40)). <sup>13</sup>C-<sup>13</sup>C “TOtal Correlated Spectroscopy” (TOCSY) NMR measurements in solution were performed on a sample containing 0.33 mM uniformly <sup>13</sup>C, <sup>15</sup>N labeled huPrP(23–144) monomers (Rösener *et al.* (40)) with 0.02% (w/v) NaN<sub>3</sub> in 30 mM HEPES buffer and 10% (v/v) D<sub>2</sub>O (pH 6.7) and on a sample of 95  $\mu$ M uniformly <sup>13</sup>C, <sup>15</sup>N labeled A $\beta$ (1–42) (Isoloid GmbH) in 30 mM Tris-HCl buffer and 10% (v/v) D<sub>2</sub>O (pH 7.2) at a temperature of 5.0 °C.

#### Solid-state NMR experiments

The solid-state NMR measurements were performed either on Varian INOVA NMR spectrometers operating at field strengths of 14.1 T ( $\omega(^1\text{H})/(2\pi) = 600$  MHz) for samples huPrP(23–144)\*-A $\beta$ , huPrP(23–230)\*-A $\beta$  and huPrP(23–144)-A $\beta$ \* or a Bruker AEON 18.8 T ( $\omega(^1\text{H})/(2\pi) = 800$  MHz) spectrometer for sample huPrP(23–144)<sub>exc</sub>-A $\beta$ \*, equipped with 3.2 mm standard (Varian) or wide bore (Bruker) triple-resonance MAS probes. Therefore either 3.2 mm thick wall (25  $\mu$ l, for samples huPrP(23–144)\*-A $\beta$  and huPrP(23–230)\*-A $\beta$ ) or thin wall (36  $\mu$ l, for sample huPrP(23–144)-A $\beta$ \*) rotors from Varian (Agilent) or 3.2 mm thick wall (46.7  $\mu$ l, for sample huPrP(23–144)<sub>exc</sub>-A $\beta$ \*) rotors from Bruker were used. For sample huPrP(23–230)\*-A $\beta$  an insert (signal at  $\approx$ 90 ppm) was used as a precaution because at the beginning of the study

it was not known if PrP in huPrP(23–230)\*-A $\beta$  was present in its pathogenic PrP<sup>Sc</sup> conformation.

Sample temperatures were indirectly determined with an accuracy of  $\pm$ 5 °C for each spinning speed using nickelocene as an external reference (74). Initial magnetization transfer from protons to <sup>13</sup>C or <sup>15</sup>N was either achieved by “insensitive nuclei enhanced by polarization transfer” (INEPT) (75) to selectively excite mobile regions *via* scalar coupling through bond magnetization transfer from <sup>1</sup>H to <sup>13</sup>C (at  $\approx$ 20, 27, or 30 °C) or by CP (measured at  $\approx$ 30, 10, 7, 0, –6, or –10 °C) *via* dipolar coupling through space transfer for rigid parts. DE experiments for sample huPrP(23–230)\*-A $\beta$  were conducted at  $\approx$ 30, 10, and –10 °C. In this temperature range, the free water in the samples was not fully frozen, as could be observed from the water signal in <sup>1</sup>H spectra (not shown). Additionally, several multidimensional homo- and heteronuclear correlation experiments for the assignment were recorded. Experimental details of all spectra recorded are given in Tables S2–S6. For homonuclear <sup>13</sup>C-<sup>13</sup>C spectra, proton-driven spin diffusion (PDS) (76) with mixing times between 10 and 300 ms was employed. Homonuclear double quantum correlation spectra were recorded with SPC5 recoupling (77).

For site-specific assignment <sup>15</sup>N-<sup>13</sup>C correlation spectra were recorded using SPECIFIC-CP (78) for frequency selective polarization transfer from <sup>15</sup>N to either <sup>13</sup>C $\alpha$  or <sup>13</sup>CO and subsequent DARR-mixing. 2D NCA, NCACX and 3D NCACX and NCOCX spectra were used for the sequential walk through the backbone. During all acquisition and evolution times, high-power broadband proton decoupling with SPINAL phase modulation (79) (radio frequency intensity between 71 and 91 kHz) was used. All spectra were processed with NMRPipe (80) with either squared and shifted sine bell or Gaussian window functions. The line width (FWHM) was estimated in 1D-slices (spectra processed with squared sine bell shifted by 0.35 $\pi$  or 0.40 $\pi$ ) of 2D PDS or NCACX/NCOCX spectra. <sup>13</sup>C chemical shifts were externally referenced with adamantane by setting the low-frequency signal of adamantane to 31.4 ppm on the DSS reference scale. <sup>15</sup>N chemical shifts were indirectly referenced *via* the <sup>13</sup>C chemical shifts. All resonances were assigned in CCPN (81). Integration of A $\beta$  peaks was done in Topspin *via* the box sum method in a PDS spectrum of huPrP(23–144)-A $\beta$ \*, measured at a temperature of  $\approx$ 0 °C, a spinning frequency of 11 kHz, and a mixing time of 50 ms.

#### Solution NMR experiments

For the sequence-specific backbone resonance assignments of uniformly <sup>13</sup>C, <sup>15</sup>N labeled huPrP(23–144) in solution at pH 4.5, the following experiments were recorded at 5.0 °C on a Bruker AVANCE III HD 600 MHz NMR spectrometer equipped with an inverse triple-resonance probe: 2D <sup>1</sup>H-<sup>15</sup>N HSQC (82), 3D HNCO (83), and 3D HNCACB (84) (further experimental details are given in Table S7). Sequence-specific backbone resonance assignments at pH 7.0 were obtained from 2D <sup>1</sup>H-<sup>15</sup>N HSQC (82), 3D HNCO (83), 3D HNCACB (84), and 3D BEST-TROSY-(H)N(COCA)NH (85)

## Solid-state MAS NMR of the complex of huPrP and A $\beta$ <sub>oligo</sub>

experiments recorded at 5.0 °C on a Varian VNMRS 800 MHz NMR spectrometer equipped with an inverse triple-resonance probe. Two 2D <sup>13</sup>C-<sup>13</sup>C TOCSY spectra covering either the aliphatic (bandwidth 70 ppm) or full (bandwidth 182 ppm) spectral region with a 13.6 ms 13.9 kHz (aliphatic) or 21.1 ms 15.6 kHz (full) FLOPSY-16 isotropic mixing scheme (86) of 0.33 mM uniformly <sup>13</sup>C, <sup>15</sup>N labeled huPrP(23–144) at 5.0 °C was recorded on a Bruker AVANCE III HD 700 MHz NMR spectrometer equipped with an inverse triple-resonance probe. Because of the comparatively low protein concentration, a 2D <sup>13</sup>C-<sup>13</sup>C TOCSY spectrum covering the aliphatic region (bandwidth 70 ppm) with a 15.1 ms 15.6 kHz FLOPSY-16 isotropic mixing scheme (86) of 95 μM uniformly <sup>13</sup>C, <sup>15</sup>N labeled A $\beta$ (1–42) at 5.0 °C was recorded on a Bruker AVANCE III HD 800 MHz NMR spectrometer equipped with a <sup>13</sup>C/<sup>15</sup>N observe triple-resonance probe; a total of 1536 transients was collected over the course of 3 weeks and added up to further improve the signal-to-noise ratio. All triple-resonance probes were cryogenically cooled and equipped with z axis pulsed field gradient capabilities. The sample temperature was calibrated using methanol-d<sub>4</sub> (87). The <sup>1</sup>H<sub>2</sub>O resonance was suppressed by gradient coherence selection with water flip-back (88), with quadrature detection in the indirect dimensions achieved by States-TPPI (89) and the echo-antiecho method (90, 91). All solution NMR spectra were processed with NMRPipe (80) software and analyzed with NMRViewJ (92) and CCPN (81). <sup>1</sup>H chemical shifts were referenced with respect to external DSS in D<sub>2</sub>O, <sup>13</sup>C and <sup>15</sup>N chemical shifts were referenced indirectly (93). RCI (50) backbone order parameters, S<sub>RCI</sub><sup>2</sup>, were calculated from the backbone chemical shifts using TALOS-N (94) with the default parameters.

To obtain sequence-specific backbone resonance assignments for huPrP(23–144) at different pH values ranging from 4.5 to 7.0 and at a temperature of 5.0 °C, we employed the following strategy: (i) In the first step, as many resonance assignments as possible (see above) were transferred from huPrP(23–230) to the <sup>1</sup>H-<sup>15</sup>N HSQC spectrum of huPrP(23–144) at pH 4.5 and 20.0 °C. (ii) Next, these resonance assignments were propagated along a temperature series of <sup>1</sup>H-<sup>15</sup>N HSQC spectra of huPrP(23–144) at pH 4.5 recorded at temperatures of 15.0 °C, 10.0 °C, and 5.0 °C. (iii) The resulting sequence-specific backbone resonance assignments at pH 4.5 and 5.0 °C were verified and completed using HNCO and HNCACB triple-resonance experiments. (iv) These resonance assignments were then propagated along a pH series of <sup>1</sup>H-<sup>15</sup>N HSQC spectra of huPrP(23–144) recorded at pH values of 5.3, 6.0, and 7.0 at a temperature of 5.0 °C. (v) Finally, the resulting sequence-specific backbone resonance assignments at pH 7.0 and 5.0 °C were verified and completed using HNCO, HNCACB, and BEST-TROSY-(H)N(COCA)NH triple-resonance experiments (Fig. S2).

### Data availability

The assigned chemical shifts of huPrP(23–144) at pH 4.5 and pH 7.0 have been deposited with the Biological Magnetic

Resonance Data Bank (BMRB) under accession codes 28115 and 28116, respectively.

**Supporting information**—This article contains supporting information (13, 19, 24–27, 32–34, 40, 41, 47, 48, 53–55, 75–78, 95–99).

**Acknowledgments**—The authors acknowledge access to the Jülich-Düsseldorf Biomolecular NMR Center that is jointly run by the Forschungszentrum Jülich and Heinrich-Heine-University Düsseldorf. The 800 MHz <sup>13</sup>C/<sup>15</sup>N observe cryoprobe was funded by a grant from the German Research Foundation (DFG INST 208/620-1 FUGG) to D. W. L. G. and D. W. acknowledge support from the Russian Science Foundation (RSF) (project no. 20-64-46027) for sample preparation. This work was supported by the Entrepreneur Foundation at the Heinrich-Heine-University of Düsseldorf and the DFG (HE 3243/4-1).

**Author contributions**—L. G. and H. H. conceived the project and designed the experiments. A. S. K., N. S. R., E. R., M. T., P. N., and L. G. performed the experiments, A. S. K., D. F., P. N., and H. H. analyzed the data. A. S. K., D. W., and H. H. wrote the article with input from all the authors. All the authors discussed the results and commented on the article.

**Funding and additional information**—Support from a European Research Council (ERC) Consolidator Grant (grant agreement no. 726368) to W. H. is acknowledged.

**Conflict of interest**—The authors declare that they have no conflicts of interest with the contents of this article.

**Abbreviations**—The abbreviations used are: A $\beta$ , amyloid  $\beta$ ; AD, Alzheimer's disease; CP, cross polarization; DE, direct excitation; INEPT, insensitive nuclei enhancement by polarization transfer; PDSO, proton-driven spin-diffusion; PrP<sup>C</sup>, cellular prion protein; RCI, Random Coil Index.

### References

- 2018 Alzheimer's disease facts and figures. *Alzheimers Dement.* **14**, (2018), 367–429
- Selkoe, D. J., and Hardy, J. (2016) The amyloid hypothesis of Alzheimer's disease at 25 years. *EMBO Mol. Med.* **8**, 595–608
- Kellett, K. A. B., and Hooper, N. M. (2009) Prion protein and Alzheimer disease. *Prion* **3**, 190–194
- Selkoe, D. J. (2008) Soluble oligomers of the amyloid  $\beta$ -protein impair synaptic plasticity and behavior. *Behav. Brain Res.* **192**, 106–113
- Lopez del Amo, J. M., Fink, U., Dasari, M., Grelle, G., Wanker, E. E., Bieschke, J., and Reif, B. (2012) Structural properties of EGCG-induced, nontoxic Alzheimer's disease A $\beta$  oligomers. *J. Mol. Biol.* **421**, 517–524
- Scheidt, H. A., Morgado, I., Rothemund, S., Huster, D., and Fandrich, M. (2011) Solid-state NMR spectroscopic investigation of Abeta protofibrils: Implication of a beta-sheet remodeling upon maturation into terminal amyloid fibrils. *Angew. Chem. Int. Ed. Engl.* **50**, 2837–2840
- Scheidt, H. A., Das, A., Korn, A., Krueger, M., Maiti, S., and Huster, D. (2020) Structural characteristics of oligomers formed by pyroglutamate-modified amyloid  $\beta$  peptides studied by solid-state NMR. *Phys. Chem. Chem. Phys.* **22**, 16887–16895
- Chimon, S., Shaibat, M. A., Jones, C. R., Calero, D. C., Aizezi, B., and Ishii, Y. (2007) Evidence of fibril-like  $\beta$ -sheet structures in a neurotoxic

- amyloid intermediate of Alzheimer's  $\beta$ -amyloid. *Nat. Struct. Mol. Biol.* **14**, 1157–1164
9. Parthasarathy, S., Inoue, M., Xiao, Y., Matsumura, Y., Nabeshima, Y.-i., Hoshi, M., and Ishii, Y. (2015) Structural insight into an Alzheimer's brain-derived spherical assembly of amyloid  $\beta$  by solid-state NMR. *J. Am. Chem. Soc.* **137**, 6480–6483
  10. Xiao, Y., Matsuda, I., Inoue, M., Sasahara, T., Hoshi, M., and Ishii, Y. (2020) NMR-based site-resolved profiling of  $\beta$ -amyloid misfolding reveals structural transitions from pathologically relevant spherical oligomer to fibril. *J. Biol. Chem.* **295**, 458–467
  11. Gao, Y., Guo, C., Watzlawik, J. O., Randolph, P. S., Lee, E. J., Huang, D., Stagg, S. M., Zhou, H.-X., Rosenberry, T. L., and Paravastu, A. K. (2020) Out-of-register parallel  $\beta$ -sheets and antiparallel  $\beta$ -sheets coexist in 150-kDa oligomers formed by amyloid- $\beta$ (1–42). *J. Mol. Biol.* **432**, 4388–4407
  12. Ahmed, M., Davis, J., Aucoin, D., Sato, T., Ahuja, S., Aimoto, S., Elliott, J. I., Van Nostrand, W. E., and Smith, S. O. (2010) Structural conversion of neurotoxic amyloid-beta(1-42) oligomers to fibrils. *Nat. Struct. Mol. Biol.* **17**, 561–567
  13. Lendel, C., Bjerring, M., Dubnovitsky, A., Kelly, R. T., Filippov, A., Antzutkin, O. N., Nielsen, N. C., and Härd, T. (2014) A hexameric peptide barrel as building block of amyloid- $\beta$  protofibrils. *Angew. Chem. Int. Ed. Engl.* **53**, 12756–12760
  14. Tay, W. M., Huang, D., Rosenberry, T. L., and Paravastu, A. K. (2013) The Alzheimer's amyloid- $\beta$ (1–42) peptide forms off-pathway oligomers and fibrils that are distinguished structurally by intermolecular organization. *J. Mol. Biol.* **425**, 2494–2508
  15. Sahoo, B. R., Cox, S. J., and Ramamoorthy, A. (2020) High-resolution probing of early events in amyloid- $\beta$  aggregation related to Alzheimer's disease. *Chem. Commun.* **56**, 4627–4639
  16. Jaroniec, C. P. (2019) Two decades of progress in structural and dynamic studies of amyloids by solid-state NMR. *J. Magn. Reson.* **306**, 42–47
  17. Li, D., and Liu, C. (2020) Structural diversity of amyloid fibrils and advances in their structure determination. *Biochemistry* **59**, 639–646
  18. Ciudad, S., Puig, E., Botzanowski, T., Meigooni, M., Arango, A. S., Do, J., Mayzel, M., Bayoumi, M., Chaignepain, S., Maglia, G., Cianferani, S., Orekhov, V., Tajkhorshid, E., Bardiaux, B., and Carulla, N. (2020) A $\beta$ (1–42) tetramer and octamer structures reveal edge conductivity pores as a mechanism for membrane damage. *Nat. Commun.* **11**, 3014
  19. Lauren, J., Gimbel, D. A., Nygaard, H. B., Gilbert, J. W., and Strittmatter, S. M. (2009) Cellular prion protein mediates impairment of synaptic plasticity by amyloid- $\beta$  oligomers. *Nature* **457**, 1128–1132
  20. Zou, W.-Q., Xiao, X., Yuan, J., Puoti, G., Fujioka, H., Wang, X., Richardson, S., Zhou, X., Zou, R., Li, S., Zhu, X., McGeer, P. L., McGeehan, J., Kneale, G., Rincon-Limas, D. E., et al. (2011) Amyloid- $\beta$ 42 interacts mainly with insoluble prion protein in the Alzheimer brain. *J. Biol. Chem.* **286**, 15095–15105
  21. Bove-Fenderson, E., Urano, R., Straub, J. E., and Harris, D. A. (2017) Cellular prion protein targets amyloid-beta fibril ends via its C-terminal domain to prevent elongation. *J. Biol. Chem.* **292**, 16858–16871
  22. Amin, L., and Harris, D. A. (2019) A $\beta$  receptors specifically recognize molecular features displayed by fibril ends and neurotoxic oligomers. *bioRxiv*. <https://doi.org/10.1101/822361>
  23. Nicoll, A. J., Panico, S., Freir, D. B., Wright, D., Terry, C., Risse, E., Herron, C. E., O'Malley, T., Wadsworth, J. D., Farrow, M. A., Walsh, D. M., Saibil, H. R., and Collinge, J. (2013) Amyloid-beta nanotubes are associated with prion protein-dependent synaptotoxicity. *Nat. Commun.* **4**, 2416
  24. Bate, C., and Williams, A. (2011) Amyloid- $\beta$ -induced synapse damage is mediated via cross-linkage of cellular prion proteins. *J. Biol. Chem.* **286**, 37955–37963
  25. Barry, A. E., Klyubin, I., McDonald, J. M., Mably, A. J., Farrell, M. A., Scott, M., Walsh, D. M., and Rowan, M. J. (2011) Alzheimer's disease brain-derived amyloid- $\beta$ -mediated inhibition of LTP *in vivo* is prevented by immunotargeting cellular prion protein. *J. Neurosci.* **31**, 7259–7263
  26. Um, J. W., Nygaard, H. B., Heiss, J. K., Kostylev, M. A., Stagi, M., Vortmeyer, A., Wisniewski, T., Gunther, E. C., and Strittmatter, S. M. (2012) Alzheimer amyloid- $\beta$  oligomer bound to postsynaptic prion protein activates Fyn to impair neurons. *Nat. Neurosci.* **15**, 1227–1235
  27. Um, J. W., and Strittmatter, S. M. (2013) Amyloid- $\beta$  induced signaling by cellular prion protein and Fyn kinase in Alzheimer disease. *Prion* **7**, 37–41
  28. Balducci, C., Beeg, M., Stravalaci, M., Bastone, A., Sclip, A., Biasini, E., Tapella, L., Colombo, L., Manzoni, C., Borsello, T., Chiesa, R., Gobbi, M., Salmona, M., and Forloni, G. (2010) Synthetic amyloid- $\beta$  oligomers impair long-term memory independently of cellular prion protein. *Proc. Natl. Acad. Sci. U. S. A.* **107**, 2295–2300
  29. Calella, A. M., Farinelli, M., Nuvolone, M., Mirante, O., Moos, R., Falsig, J., Mansuy, I. M., and Aguzzi, A. (2010) Prion protein and A $\beta$ -related synaptic toxicity impairment. *EMBO Mol. Med.* **2**, 306–314
  30. Kessels, H. W., Nguyen, L. N., Nabavi, S., and Malinow, R. (2010) The prion protein as a receptor for amyloid- $\beta$ . *Nature* **466**, E3–E4
  31. Cissé, M., Sanchez, P. E., Kim, D. H., Ho, K., Yu, G.-Q., and Mucke, L. (2011) Ablation of cellular prion protein does not ameliorate abnormal neural network activity or cognitive dysfunction in the J20 line of human amyloid precursor protein transgenic mice. *J. Neurosci.* **31**, 10427–10431
  32. Nieznanski, K., Choi, J.-K., Chen, S., Surewicz, K., and Surewicz, W. K. (2012) Soluble prion protein inhibits amyloid- $\beta$  (A $\beta$ ) fibrillization and toxicity. *J. Biol. Chem.* **287**, 33104–33108
  33. Mohammadi, B., Linsenmeier, L., Shafiq, M., Puig, B., Galliciotti, G., Giudici, C., Willem, M., Eden, T., Koch-Nolte, F., Lin, Y.-H., Tatzelt, J., Glatzel, M., and Altmepfen, H. C. (2020) Transgenic overexpression of the disordered prion protein N1 fragment in mice does not protect against neurodegenerative diseases due to impaired ER translocation. *Mol. Neurobiol.* **57**, 2812–2829
  34. Guillot-Sestier, M.-V., Sunyach, C., Ferreira, S. T., Marzolo, M.-P., Bauer, C., Thevenet, A., and Checler, F. (2012)  $\alpha$ -Secretase-derived fragment of cellular prion, N1, protects against monomeric and oligomeric amyloid  $\beta$  (A $\beta$ )-associated cell death. *J. Biol. Chem.* **287**, 5021–5032
  35. Chen, S., Yadav, S. P., and Surewicz, W. K. (2010) Interaction between human prion protein and amyloid- $\beta$  (A $\beta$ ) oligomers: Role of N-terminal residues. *J. Biol. Chem.* **285**, 26377–26383
  36. Fluharty, B. R., Biasini, E., Stravalaci, M., Sclip, A., Diomedea, L., Balducci, C., La Vitola, P., Messa, M., Colombo, L., Forloni, G., Borsello, T., Gobbi, M., and Harris, D. A. (2013) An N-terminal fragment of the prion protein binds to amyloid-beta oligomers and inhibits their neurotoxicity *in vivo*. *J. Biol. Chem.* **288**, 7857–7866
  37. Kang, M., Kim, S. Y., An, S. S., and Ju, Y. R. (2013) Characterizing affinity epitopes between prion protein and beta-amyloid using an epitope mapping immunoassay. *Exp. Mol. Med.* **45**, e34
  38. Dohler, F., Sepulveda-Falla, D., Krasemann, S., Altmepfen, H., Schlüter, H., Hildebrand, D., Zerr, I., Matschke, J., and Glatzel, M. (2014) High molecular mass assemblies of amyloid- $\beta$  oligomers bind prion protein in patients with Alzheimer's disease. *Brain* **137**, 873–886
  39. Younan, N. D., Sarell, C. J., Davies, P., Brown, D. R., and Viles, J. H. (2013) The cellular prion protein traps Alzheimer's A $\beta$  in an oligomeric form and disassembles amyloid fibers. *FASEB J.* **27**, 1847–1858
  40. Rösener, N. S., Gremer, L., Reinartz, E., König, A., Brener, O., Heise, H., Hoyer, W., Neudecker, P., and Willbold, D. (2018) A d-enantiomeric peptide interferes with heteroassociation of amyloid- $\beta$  oligomers and prion protein. *J. Biol. Chem.* **293**, 15748–15764
  41. Rösener, N. S., Gremer, L., Wördehoff, M. M., Kupreichyk, T., Etkorn, M., Neudecker, P., and Hoyer, W. (2020) Clustering of human prion protein and  $\alpha$ -synuclein oligomers requires the prion protein N-terminus. *Commun. Biol.* **3**, 365
  42. Corbett, G. T., Wang, Z., Hong, W., Colom-Cadena, M., Rose, J., Liao, M., Asfaw, A., Hall, T. C., Ding, L., DeSousa, A., Frosch, M. P., Collinge, J., Harris, D. A., Perkinson, M. S., Spires-Jones, T. L., et al. (2020) PrP is a central player in toxicity mediated by soluble aggregates of neurodegeneration-causing proteins. *Acta Neuropathol.* **139**, 503–526
  43. Ferreira, D. G., Temido-Ferreira, M., Miranda, H. V., Batalha, V. L., Coelho, J. E., Szegő, É. M., Marques-Morgado, I., Vaz, S. H., Rhee, J. S., and Schmitz, M. (2017)  $\alpha$ -synuclein interacts with PrP C to induce cognitive impairment through mGluR5 and NMDAR2B. *Nat. Neurosci.* **20**, 1569
  44. Kostylev, M. A., Tuttle, M. D., Lee, S., Klein, L. E., Takahashi, H., Cox, T. O., Gunther, E. C., Zilm, K. W., and Strittmatter, S. M. (2018) Liquid and hydrogel phases of PrP(C) linked to conformational shifts and triggered by Alzheimer's amyloid-beta oligomers. *Mol. Cell* **72**, 426–443.e012
  45. Colvin, M. T., Silvers, R., Ni, Q. Z., Can, T. V., Sergeev, I., Rosay, M., Donovan, K. J., Michael, B., Wall, J., Linse, S., and Griffin, R. G. (2016)

- Atomic resolution structure of monomeric A $\beta$ 42 amyloid fibrils. *J. Am. Chem. Soc.* **138**, 9663–9674
46. Wälti, M. A., Ravotti, F., Arai, H., Glabe, C. G., Wall, J. S., Böckmann, A., Güntert, P., Meier, B. H., and Riek, R. (2016) Atomic-resolution structure of a disease-relevant A $\beta$ (1–42) amyloid fibril. *Proc. Natl. Acad. Sci. U. S. A.* **113**, E4976–E4984
  47. Gremer, L., Schölzel, D., Schenk, C., Reinartz, E., Labahn, J., Ravelli, R. B. G., Tusche, M., Lopez-Iglesias, C., Hoyer, W., Heise, H., Willbold, D., and Schröder, G. F. (2017) Fibril structure of amyloid- $\beta$ (1–42) by cryo-electron microscopy. *Science* **358**, 116–119
  48. Zahn, R., Liu, A., Lührs, T., Riek, R., von Schroetter, C., López García, F., Billeter, M., Calzolari, L., Wider, G., and Wüthrich, K. (2000) NMR solution structure of the human prion protein. *Proc. Natl. Acad. Sci. U. S. A.* **97**, 145–150
  49. Wishart, D. S., Bigam, C. G., Holm, A., Hodges, R. S., and Sykes, B. D. (1995) H-1, C-13 and N-15 random coil NMR chemical-shifts of the common amino-acids.1. Investigations of nearest-neighbor effects. *J. Biomol. NMR* **5**, 67–81
  50. Berjanskii, M. V., and Wishart, D. S. (2005) A simple method to predict protein flexibility using secondary chemical shifts. *J. Am. Chem. Soc.* **127**, 14970–14971
  51. Andronesi, O. C., Becker, S., Seidel, K., Heise, H., Young, H. S., and Baldus, M. (2005) Determination of membrane protein structure and dynamics by magic-angle-spinning solid-state NMR spectroscopy. *J. Am. Chem. Soc.* **127**, 12965–12974
  52. Helmus, J. J., Surewicz, K., Nadaud, P. S., Surewicz, W. K., and Jaroniec, C. P. (2008) Molecular conformation and dynamics of the Y145Stop variant of human prion protein in amyloid fibrils. *Proc. Natl. Acad. Sci. U. S. A.* **105**, 6284–6289
  53. Theint, T., Nadaud, P. S., Surewicz, K., Surewicz, W. K., and Jaroniec, C. P. (2017) <sup>13</sup>C and <sup>15</sup>N chemical shift assignments of mammalian Y145Stop prion protein amyloid fibrils. *Biomol. NMR Assign.* **11**, 75–80
  54. Glynn, C., Sawaya, M. R., Ge, P., Gallagher-Jones, M., Short, C. W., Bowman, R., Apostol, M., Zhou, Z. H., Eisenberg, D. S., and Rodriguez, J. A. (2020) Cryo-EM structure of a human prion fibril with a hydrophobic, protease-resistant core. *Nat. Struct. Mol. Biol.* **27**, 417–423
  55. Wang, L.-Q., Zhao, K., Yuan, H.-Y., Wang, Q., Guan, Z., Tao, J., Li, X.-N., Sun, Y., Yi, C.-W., Chen, J., Li, D., Zhang, D., Yin, P., Liu, C., and Liang, Y. (2020) Cryo-EM structure of an amyloid fibril formed by full-length human prion protein. *Nat. Struct. Mol. Biol.* **27**, 598–602
  56. Pagano, K., Galante, D., D'Arrigo, C., Corsaro, A., Nizzari, M., Florio, T., Molinari, H., Tomaselli, S., and Ragona, L. (2019) Effects of prion protein on A $\beta$ 42 and pyroglutamate-modified A $\beta$ pE3-42 oligomerization and toxicity. *Mol. Neurobiol.* **56**, 1957–1971
  57. You, H., Tsutsui, S., Hameed, S., Kannanayakal, T. J., Chen, L., Xia, P., Engbers, J. D. T., Lipton, S. A., Stys, P. K., and Zamponi, G. W. (2012) A $\beta$  neurotoxicity depends on interactions between copper ions, prion protein, and N-methyl-D-aspartate receptors. *Proc. Natl. Acad. Sci. U. S. A.* **109**, 1737–1742
  58. Williams, T. L., Choi, J.-K., Surewicz, K., and Surewicz, W. K. (2015) Soluble prion protein binds isolated low molecular weight amyloid- $\beta$  oligomers causing cytotoxicity inhibition. *ACS Chem. Neurosci.* **6**, 1972–1980
  59. Kostylev, M. A., Kaufman, A. C., Nygaard, H. B., Patel, P., Haas, L. T., Gunther, E. C., Vortmeyer, A., and Strittmatter, S. M. (2015) Prion-protein-interacting amyloid- $\beta$  oligomers of high molecular weight are tightly correlated with memory impairment in multiple Alzheimer mouse models. *J. Biol. Chem.* **290**, 17415–17438
  60. Madhu, P., and Mukhopadhyay, S. (2020) Preferential recruitment of conformationally distinct amyloid- $\beta$  oligomers by the intrinsically disordered region of the human prion protein. *ACS Chem. Neurosci.* **11**, 86–98
  61. Brener, O., Dunkelmann, T., Gremer, L., van Groen, T., Mirecka, E. A., Kadish, I., Willuweit, A., Kutzsche, J., Jürgens, D., Rudolph, S., Tusche, M., Bongen, P., Pietruszka, J., Oesterheld, F., Langen, K.-J., et al. (2015) QIAD assay for quantitating a compound's efficacy in elimination of toxic A $\beta$  oligomers. *Sci. Rep.* **5**, 13222–13234
  62. Freir, D. B., Nicoll, A. J., Klyubin, I., Panico, S., Mc Donald, J. M., Risse, E., Asante, E. A., Farrow, M. A., Sessions, R. B., Saibil, H. R., Clarke, A. R., Rowan, M. J., Walsh, D. M., and Collinge, J. (2011) Interaction between prion protein and toxic amyloid  $\beta$  assemblies can be therapeutically targeted at multiple sites. *Nat. Commun.* **2**, 336
  63. Kudo, W., Lee, H.-P., Zou, W.-Q., Wang, X., Perry, G., Zhu, X., Smith, M. A., Petersen, R. B., and Lee, H.-g. (2012) Cellular prion protein is essential for oligomeric amyloid- $\beta$ -induced neuronal cell death. *Hum. Mol. Genet.* **21**, 1138–1144
  64. Peters, C., Espinoza, M. P., Gallegos, S., Opazo, C., and Aguayo, L. G. (2015) Alzheimer's A $\beta$  interacts with cellular prion protein inducing neuronal membrane damage and synaptotoxicity. *Neurobiol. Aging* **36**, 1369–1377
  65. Silvers, R., Colvin, M. T., Frederick, K. K., Jacavone, A. C., Lindquist, S., Linse, S., and Griffin, R. G. (2017) Aggregation and fibril structure of A $\beta$ M01–42 and A $\beta$ 1–42. *Biochemistry* **56**, 4850–4859
  66. Gasset, M., Baldwin, M. A., Lloyd, D. H., Gabriel, J. M., Holtzman, D. M., Cohen, F., Fletterick, R., and Prusiner, S. B. (1992) Predicted alpha-helical regions of the prion protein when synthesized as peptides form amyloid. *Proc. Natl. Acad. Sci. U. S. A.* **89**, 10940–10944
  67. Norstrom, E. M., and Mastrianni, J. A. (2005) The AGAAAAGA palindrome in PrP is required to generate a productive PrPSc-PrPC complex that leads to prion propagation. *J. Biol. Chem.* **280**, 27236–27243
  68. Sarell, C. J., Quarterman, E., Yip, D. C., Terry, C., Nicoll, A. J., Wadsworth, J. D. F., Farrow, M. A., Walsh, D. M., and Collinge, J. (2017) Soluble Abeta aggregates can inhibit prion propagation. *Open Biol.* **7**, 170158
  69. Um, J. W., Kaufman, A. C., Kostylev, M., Heiss, J. K., Stagi, M., Takahashi, H., Kerrisk, M. E., Vortmeyer, A., Wisniewski, T., Koleske, A. J., Gunther, E. C., Nygaard, H. B., and Strittmatter, S. M. (2013) Metabotropic glutamate receptor 5 is a coreceptor for Alzheimer A $\beta$  oligomer bound to cellular prion protein. *Neuron* **79**, 887–902
  70. Hu, N.-W., Nicoll, A. J., Zhang, D., Mably, A. J., O'Malley, T., Purro, S. A., Terry, C., Collinge, J., Walsh, D. M., and Rowan, M. J. (2014) mGlu5 receptors and cellular prion protein mediate amyloid- $\beta$ -facilitated synaptic long-term depression *in vivo*. *Nat. Commun.* **5**, 3374
  71. Haas, L. T., Salazar, S. V., Kostylev, M. A., Um, J. W., Kaufman, A. C., and Strittmatter, S. M. (2016) Metabotropic glutamate receptor 5 couples cellular prion protein to intracellular signalling in Alzheimer's disease. *Brain* **139**, 526–546
  72. Potapov, A., Yau, W. M., Ghirlando, R., Thurber, K. R., and Tycko, R. (2015) Successive stages of amyloid-beta self-assembly characterized by solid-state nuclear magnetic resonance with dynamic nuclear polarization. *J. Am. Chem. Soc.* **137**, 8294–8307
  73. Mengel, D., Hong, W., Corbett, G. T., Liu, W., DeSousa, A., Solfrosi, L., Fang, C., Frosch, M. P., Collinge, J., Harris, D. A., and Walsh, D. M. (2019) PrP-grafted antibodies bind certain amyloid  $\beta$ -protein aggregates, but do not prevent toxicity. *Brain Res.* **1710**, 125–135
  74. Heise, H., Köhler, F. H., and Xie, X. L. (2001) Solid-state NMR spectroscopy of paramagnetic metalocenes. *J. Magn. Reson.* **150**, 198–206
  75. Morris, G. A., and Freeman, R. (1979) Enhancement of nuclear magnetic resonance signals by polarization transfer. *J. Am. Chem. Soc.* **101**, 760–762
  76. Szeverenyi, N. M., Sullivan, M. J., and Maciel, G. E. (1982) Observation of spin exchange by two-dimensional Fourier transform <sup>13</sup>C cross polarization-magic-angle spinning. *J. Magn. Reson.* (1969) **47**, 462–475
  77. Hohwy, M., Rienstra, C. M., Jaroniec, C. P., and Griffin, R. G. (1999) Fivefold symmetric homonuclear dipolar recoupling in rotating solids: Application to double quantum spectroscopy. *J. Chem. Phys.* **110**, 7983–7992
  78. Baldus, M., Petkova, A. T., Herzfeld, J., and Griffin, R. G. (1998) Cross polarization in the tilted frame: Assignment and spectral simplification in heteronuclear spin systems. *Mol. Phys.* **95**, 1197–1207
  79. Fung, B. M., Khitrin, A. K., and Ermolaev, K. (2000) An improved broadband decoupling sequence for liquid crystals and solids. *J. Magn. Reson.* **142**, 97–101
  80. Delaglio, F., Grzesiek, S., Vuister, G. W., Zhu, G., Pfeifer, J., and Bax, A. (1995) NMRPipe: A multidimensional spectral processing system based on UNIX pipes. *J. Biomol. NMR* **6**, 277–293
  81. Skinner, S. P., Fogh, R. H., Boucher, W., Ragan, T. J., Mureddu, L. G., and Vuister, G. W. (2016) CcpNmr AnalysisAssign: A flexible platform for integrated NMR analysis. *J. Biomol. NMR* **66**, 111–124

82. Zhang, O., Kay, L. E., Olivier, J. P., and Forman-Kay, J. D. (1994) Backbone <sup>1</sup>H and <sup>15</sup>N resonance assignments of the N-terminal SH3 domain of drk in folded and unfolded states using enhanced-sensitivity pulsed field gradient NMR techniques. *J. Biomol. NMR* **4**, 845–858
83. Ikura, M., Kay, L. E., and Bax, A. (1990) A novel approach for sequential assignment of <sup>1</sup>H, <sup>13</sup>C, and <sup>15</sup>N spectra of larger proteins: Heteronuclear triple-resonance three-dimensional NMR spectroscopy. Application to calmodulin. *Biochemistry* **29**, 4659–4667
84. Wittekind, M., and Mueller, L. (1993) HNCACB, a high-sensitivity 3D NMR experiment to correlate amide-proton and nitrogen resonances with the alpha- and beta-carbon resonances in proteins. *J. Magn. Reson. Ser. B* **101**, 201–205
85. Solyom, Z., Schwarten, M., Geist, L., Konrat, R., Willbold, D., and Brutscher, B. (2013) BEST-TROSY experiments for time-efficient sequential resonance assignment of large disordered proteins. *J. Biomol. NMR* **55**, 311–321
86. Kovacs, H., and Gossert, A. (2014) Improved NMR experiments with <sup>13</sup>C-isotropic mixing for assignment of aromatic and aliphatic side chains in labeled proteins. *J. Biomol. NMR* **58**, 101–112
87. Findeisen, M., Brand, T., and Berger, S. (2007) A <sup>1</sup>H-NMR thermometer suitable for cryoprobes. *Magn. Reson. Chem.* **45**, 175–178
88. Grzesiek, S., and Bax, A. (1993) The importance of not saturating water in protein NMR. Application to sensitivity enhancement and NOE measurements. *J. Am. Chem. Soc.* **115**, 12593–12594
89. Marion, D., Ikura, M., Tschudin, R., and Bax, A. (1989) Rapid recording of 2D NMR spectra without phase cycling. Application to the study of hydrogen exchange in proteins. *J. Magn. Reson. (1969)* **85**, 393–399
90. Kay, L., Keifer, P., and Saarienen, T. (1992) Pure absorption gradient enhanced heteronuclear single quantum correlation spectroscopy with improved sensitivity. *J. Am. Chem. Soc.* **114**, 10663–10665
91. Schleucher, J., Sattler, M., and Griesinger, C. (1993) Coherence selection by gradients without signal attenuation: Application to the three-dimensional HNCO experiment. *Angew. Chem. Int. Ed. Engl.* **32**, 1489–1491
92. Johnson, B. A., and Blevins, R. A. (1994) NMR view: A computer program for the visualization and analysis of NMR data. *J. Biomol. NMR* **4**, 603–614
93. Markley John, L., Bax, A., Arata, Y., Hilbers, C. W., Kaptein, R., Sykes Brian, D., Wright Peter, E., and Wüthrich, K. (1998) Recommendations for the presentation of NMR structures of proteins and nucleic acids (IUPAC recommendations 1998). *Pure Appl. Chem.* **70**, 117–142
94. Shen, Y., and Bax, A. (2013) Protein backbone and sidechain torsion angles predicted from NMR chemical shifts using artificial neural networks. *J. Biomol. NMR* **56**, 227–241
95. Han, B., Liu, Y., Ginzinger, S. W., and Wishart, D. S. (2011) SHIFTX2: Significantly improved protein chemical shift prediction. *J. Biomol. NMR* **50**, 43
96. Schulte, C. F., Tolmie, D. E., Maziuk, D., Nakatani, E., Akutsu, H., Yao, H., Markley, J. L., Lin, J., Dorelejers, J. F., Livny, M., Kent Wenger, R., Mading, S., Ioannidis, Y. E., Harano, Y., Müller, Z., et al. (2007) BioMagResBank. *Nucleic Acids Res.* **36**, D402–D408
97. Calzolari, L., and Zahn, R. (2003) Influence of pH on NMR structure and stability of the human prion protein globular domain. *J. Biol. Chem.* **278**, 35592–35596
98. Colvin, M. T., Silvers, R., Frohm, B., Su, Y., Linse, S., and Griffin, R. G. (2015) High resolution structural characterization of A $\beta$ <sub>42</sub> amyloid fibrils by magic angle spinning NMR. *J. Am. Chem. Soc.* **137**, 7509–7518
99. Ravotti, F., Wälti, M. A., Güntert, P., Riek, R., Böckmann, A., and Meier, B. H. (2016) Solid-state NMR sequential assignment of an Amyloid- $\beta$ <sub>(1–42)</sub> fibril polymorph. *Biomol. NMR Assign.* **10**, 269–276